Research Square

Preprints are preliminary reports that have not undergone peer review.
They should not be considered conclusive, used to inform clinical practice,
or referenced by the media as validated information.

Robust Single-Ended Fault Location in Double-Circuit Lines with Fault Topology Identification and Uncertainty Quantification

Abhay Yadav
Sharda University
Soma Deb
soma.deb@sharda.ac.in

Sharda University
Dr. V. P Singh
Malaviya National Institute of Technology Jaipur

Research Article

Keywords: Double-circuit transmission line, Fault location, Single-ended measurement, Distributed-parameter model, Decaying dc offset, Robust estimation, Fault classification, Confidence interval

Posted Date: November 18th, 2026

DOI: https://doi.org/10.21203/rs.3.rs-11513737/v1

License: This work is licensed under a Creative Commons Attribution 4.0 International License.
Read Full License

Additional Declarations: No competing interests reported.

Robust Single-Ended Fault Location in Double-Circuit Lines with Fault Topology Identification and Uncertainty Quantification

Abhay Yadav[1], Soma Deb[1*], V. P. Singh[2]

[1]EECE, SSES, Sharda University, Greater Noida, India.
[2]Department of Electrical Engineering, Malaviya National Institute of Technology, Jaipur, India.

*Corresponding author(s). E-mail(s): soma.deb@sharda.ac.in;
Contributing authors: 2024102693.abhay@dr.sharda.ac.in;
vinay.ee@mnit.ac.in;

Abstract

Single-ended fault location on double-circuit transmission lines is complicated by the mutual coupling between the circuits, the remote-end infeed and the decaying dc component of the fault current. This paper proposes a method in which the fault distance and the fault path conductances are estimated jointly from the condition that the remote-bus voltages calculated through the two circuits of an exact six-conductor distributed-parameter model must be equal. Thirty-one fault types, including the faulted circuit, are fitted by a weighted Huber estimator and ranked by the Bayesian information criterion; faults that cannot be located from one end are detected, and confidence intervals are obtained by Monte Carlo propagation. The phasors are estimated by a two-cycle least-squares fit that includes the decaying dc term, and instrument transformer errors and time skew between channels are corrected. The method and a recent single-ended method were applied to the same waveforms of 1658 simulated faults on a 500 kV line of 150–400 km. For the 990 noise-free cases of the main study, the median error was 0.0014 % against 0.270 %, and the fault type was identified correctly for 99.5 % of the tested observable faults. With protection-class instrument transformer errors and certificate correction, the median error was 0.071 % against 0.237 %. The coverage of the 95 % confidence interval was 98.1–100 % in all case sets. Errors in the zero-sequence impedance, an inductive fault impedance and an uncorrected current-to-voltage time skew remain the main error sources.

Keywords: Double-circuit transmission line, Fault location, Single-ended measurement, Distributed-parameter model, Decaying dc offset, Robust estimation, Fault classification, Confidence interval

1 Introduction

Double-circuit transmission lines, in which two three-phase circuits share the same towers and right-of-way, are widely used in extra-high-voltage corridors because they double the transfer capability per unit of land. Accurate fault location on these lines shortens the inspection time, accelerates the restoration of the faulted circuit and reduces the cost of the outage.

Fault location methods are generally classified into traveling-wave, knowledge-based and impedance-based methods. Traveling-wave methods determine the fault position from the arrival times of the surges launched by the fault and can be very accurate, but they require sampling rates in the megahertz range, dedicated acquisition hardware and reliable wave-front detection [1–3]. Knowledge-based methods, such as artificial neural networks, require large training sets, and their performance outside the training region cannot be guaranteed [4, 5]. Impedance-based methods use the fundamental-frequency voltage and current phasors that are already available in digital relays and disturbance recorders, which explains their wide use in practice.

Impedance-based methods are divided into single-ended and multiend methods. Among single-ended methods, the reactance method of Takagi et al. [6] eliminates the fault resistance by means of the pure fault current, and Eriksson et al. [7] compensated the apparent reactance caused by the remote-end infeed; practical aspects of these methods are discussed in [8]. Later work estimated the remote equivalent impedance adaptively [9] or formulated the problem in the time domain [10]. Two-ended methods remove the effect of the fault resistance by using synchronised or unsynchronised measurements from both terminals [11–13]. The distributed-parameter line model was introduced to account for line charging on long lines [14, 15], and further contributions include adaptive PMU-based schemes [16], noniterative two-ended formulations [17], parameter-free location on untransposed lines [18] and time-domain methods that consider the full line asymmetry [19]. Multiend methods are accurate but require a communication channel and, in most cases, time synchronisation between the terminals.

On double-circuit lines, the zero-sequence mutual coupling between the circuits is large (about 65 % of the zero-sequence self-impedance for the line studied here) and depends on the operating state of the parallel circuit; therefore, single-circuit methods cannot be applied directly. Kawady and Stenzel [20] and Izykowski et al. [21] showed that the mutual coupling can be compensated without remote data when the currents of both circuits are measured at the relay location. Single-ended methods have since been developed for parallel lines [22], lines with different configurations [23], multiterminal and shunt-compensated double-circuit lines [24, 25], series-compensated lines [26] and partially coupled lines [27]. Two-ended methods have been proposed with unsynchronised measurements [28], without line parameters [29], with series

compensation [30] and with synchronised current phasors [31]; the estimation of the zero-sequence self and mutual impedances required by these methods is addressed in [32].

Recently, Khodadadi Arpanahi et al. [33] proposed a single-ended method for double-circuit lines that uses the sending-end voltages and the currents of both circuits and represents the line by its distributed-parameter equivalent. The method alternates between the calculation of the fault-point voltages and currents for a given distance and the update of the distance from the fault loop equation of one faulted phase, and it usually converges within two or three iterations. The faulted phases are recognised after convergence from the estimated fault currents, so that the fault type is not an input; phase-to-phase faults require a modified update, and intercircuit faults require three healthy phases to be assigned to the healthy circuit. Errors mostly below 0.5 % and up to about 1 % were reported for a 400 kV line of 50–400 km. Because of its accuracy and general matrix formulation, this method is used for comparison in this paper and is referred to as the method of [33]. Data-driven fault classifiers for double-circuit lines are reported in [34–37].

The following problems remain open in the method of [33] and in related single-ended methods:

- The distance is obtained by a fixed-point iteration that uses the fault loop equation of a single faulted phase. The original update for phase-to-phase faults did not always converge in the present simulations, and the iteration does not minimise an error measure over all measured channels, so the information in the healthy phases is not used.
- The faulted phases are identified only after convergence, and no measure of the goodness of fit is available. An uncertain identification, e.g. between a single-circuit and a cross-circuit fault, therefore produces a location without any warning.
- The phasors are computed by the one-cycle discrete Fourier transform (DFT) [38], which is biased by the decaying dc component of the fault current. Many dc-robust phasor estimators exist [39–47], but they have not been integrated into double-circuit fault location.
- Only a point estimate is returned, although measurement and line parameter errors strongly affect the result [48–52], and instrument transformer errors [53] increase the error further. No confidence interval is provided.
- Least-squares formulations are sensitive to outliers, and robust estimators [49, 54, 55] have not been applied. Moreover, some fault types, such as a fault between the same phases of both circuits to ground, cannot be located from one end; a practical locator should detect such faults instead of returning a wrong distance.

The use of the common remote bus of parallel lines is not new: Kawady and Stenzel [20] and Izykowski et al. [21] eliminated the remote infeed by combining the currents of both circuits, and [22] extended this idea to parallel lines with different configurations. In this paper, a single-ended fault location method for double-circuit lines without a fixed-point distance update is proposed. It assumes that both circuits are in service and terminate at the same buses and that no circuit breaker operates within the data record. The main contributions are:

- A direct estimator in which the fault distance and the fault path conductances are obtained jointly by minimising the common-bus residual of the exact six-conductor distributed-parameter model, including mutual coupling and shunt capacitance, without a fault-type-specific update formula.
- Identification of the fault type and the faulted circuit among 31 fault types (Table 1) by the Bayesian information criterion (BIC) [56], a consistent counterpart of the Akaike criterion [57], together with an observability test that detects faults which cannot be located from one end.
- A dc-robust phasor estimator based on a two-cycle least-squares fit with an optimised time constant, combined with multiwindow fusion and a dedicated bolted-fault model.
- A weighted Huber estimator [54, 58] whose weights account for measurement noise, line parameter uncertainty and model residual, and a Monte Carlo procedure with a model bias term that gives 95 % confidence intervals with verified coverage.
- Correction of instrument transformer ratio and phase errors and joint estimation of the time skew between channels, with an identifiability test that shows for which faults the skew can be estimated from one end.
- An evaluation on 1658 fault cases of a 500 kV double-circuit line of 150–400 km and on the test cases of [33], in which both methods are applied to the same waveforms. An exact network solver, verified against Simscape Electrical, was used to make the simulation study feasible.

1.1 Organization of the paper

The rest of the paper is organized as follows:

- Section 2 describes the proposed method: the general outline (Section 2.1), the six-conductor distributed-parameter line model (Section 2.2), the phasor estimation with the decaying dc component (Section 2.3), the common-bus formulation and the estimation for each fault type (Section 2.4), and the fault type selection, observability test and confidence interval (Section 2.5).
- Section 3 presents the test system, the simulated cases and the simulation results: the effect of fault type, location and resistance (Section 3.1), line length (Section 3.2), convergence and computation time (Section 3.3), untransposed and nonidentical circuits (Section 3.4), measurement noise (Section 3.5), inception angle and sampling frequency (Section 3.6), line parameter errors (Section 3.7), fault inductance (Section 3.8), prefault loading and unseen cases (Section 3.9), and the comparison with the method of [33] (Section 3.10).
- Section 4 discusses the robustness to measurement errors (Section 4.1), the instrument transformer correction and time skew estimation (Section 4.1.1), the contribution of each part of the method (Section 4.2) and the limitations (Section 4.3).
- Section 5 concludes the paper, and Appendix A gives the distance update of the method of [33].

2 Proposed method

2.1 General outline

The proposed method uses only the measurements at the sending-end bus S: the three phase voltages of the bus and the three phase currents of each circuit. The outline of the method and the line representation are shown in Fig. 1. In contrast to [33], where two subproblems are solved alternately, the method consists of three stages that are executed once. In Stage 1, the fundamental-frequency phasors are estimated from several postfault data windows with a signal model that includes the decaying dc component. In Stage 2, the fault distance d and the fault path conductances are estimated for each of the 31 fault types by minimising a robust weighted norm of the common-bus residual over all windows. In Stage 3, the topology is selected by the BIC, the observability and uniqueness of the solution are checked, and a 95 % confidence interval is calculated. The complete procedure is given in Algorithm 1 and Fig. 2.

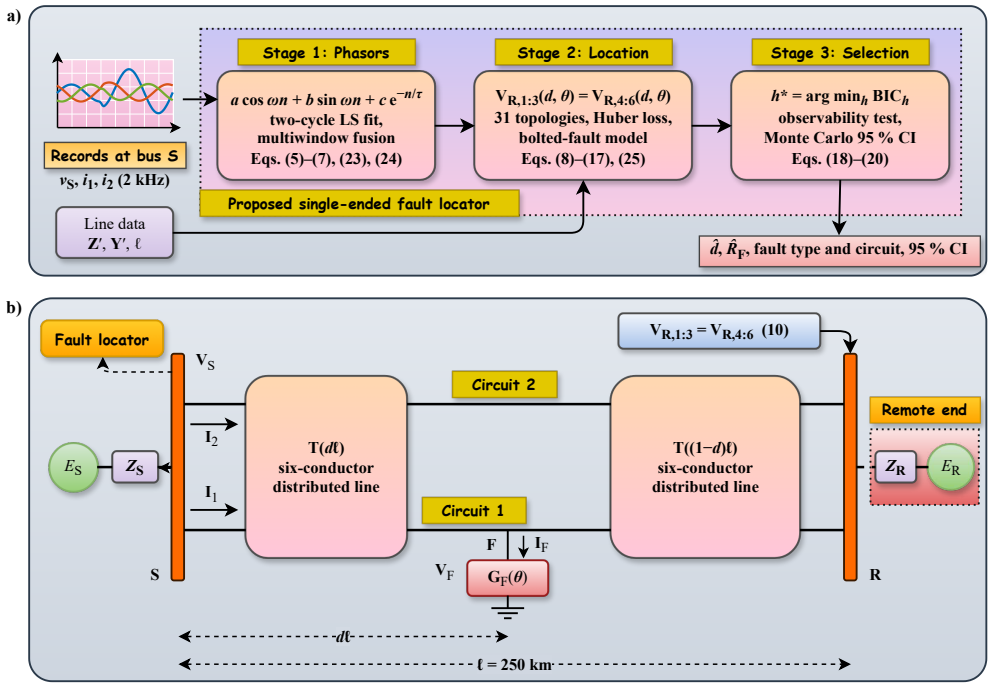


Fig. 1 Proposed method: a) outline of the three stages; b) double-circuit line with a fault at distance dℓ from bus S

2.2 Line model

The six conductors of the double-circuit line are ordered as [A1 B1 C1 A2 B2 C2], where the indices 1 and 2 denote the two circuits. The line, of length ℓ, is described by its 6×6 per-unit-length series impedance and shunt admittance matrices:

$$\mathbf{Z}' = \mathbf{R}' + j\omega\mathbf{L}', \qquad \mathbf{Y}' = j\omega\mathbf{C}' \tag{1}$$

where $\mathbf{R}'$, $\mathbf{L}'$ and $\mathbf{C}'$ are the per-unit-length resistance, inductance and capacitance matrices and ω is the fundamental angular frequency. For a line given by sequence parameters, the diagonal entries of each matrix are $(X_0 + 2X_1)/3$, the off-diagonal entries within one circuit are $(X_0 - X_1)/3$, and the entries between the circuits are $X_{0m}/3$, where X stands for R, L or C and the subscripts 1, 0 and 0m denote the positive-sequence, zero-sequence and zero-sequence mutual quantities [20, 21]. For an untransposed or nonidentical line, the full matrices are used.

Let $\mathbf{x}(z) = [\mathbf{V}(z);\ \mathbf{I}(z)] \in \mathbb{C}^{12}$ be the vector of phase voltage and current phasors at distance z from bus S. The telegrapher equations of the six-conductor line are

$$\frac{d\mathbf{x}}{dz} = \mathbf{A}\,\mathbf{x}, \qquad \mathbf{A} = \begin{bmatrix} \mathbf{0} & -\mathbf{Z}' \\ -\mathbf{Y}' & \mathbf{0} \end{bmatrix} \tag{2}$$

and their solution relates the states at both ends of a line section of length z:

$$\mathbf{x}(z) = \mathbf{T}(z)\,\mathbf{x}(0), \qquad \mathbf{T}(z) = e^{\mathbf{A}z} = \begin{bmatrix} \mathbf{T}_{VV}(z) & \mathbf{T}_{VI}(z) \\ \mathbf{T}_{IV}(z) & \mathbf{T}_{II}(z) \end{bmatrix} \tag{3}$$

where $\mathbf{T}(z)$ is the exact 12×12 chain matrix of the distributed-parameter line, calculated by the matrix exponential. Equation (3) contains no lumped π approximation and is valid for transposed, untransposed and nonidentical circuits.

The measured sending-end state is

$$\mathbf{x}_S = \begin{bmatrix} \mathbf{V}_S \\ \mathbf{I}_S \end{bmatrix}, \qquad \mathbf{V}_S = \begin{bmatrix} \mathbf{v}_S \\ \mathbf{v}_S \end{bmatrix}, \qquad \mathbf{I}_S = \begin{bmatrix} \mathbf{i}_1 \\ \mathbf{i}_2 \end{bmatrix} \tag{4}$$

where $\mathbf{v}_S \in \mathbb{C}^3$ contains the bus-S phase voltages, common to both circuits, and $\mathbf{i}_1, \mathbf{i}_2 \in \mathbb{C}^3$ are the phase currents of circuits 1 and 2 at bus S.

2.3 Stage 1: Phasor estimation with decaying dc component

A fault produces a decaying dc component in the line currents, whose amplitude is largest for low fault resistance and for inception near the voltage zero crossing [41, 42]. For the line studied in Section 3, its time constant is 22–44 ms. The one-cycle DFT [38] does not reject this component; for bolted faults, the one-cycle current phasor deviates from its steady-state value by about 6 %. Therefore, each channel x[n] (voltage or current) is modelled over a two-cycle window of 2N samples (N = 40 at f_s = 2 kHz) as

$$x[n] = a\cos(\omega n T_s) + b\sin(\omega n T_s) + c\,e^{-nT_s/\tau} + \varepsilon[n], \qquad n = 0, \ldots, 2N-1 \tag{5}$$

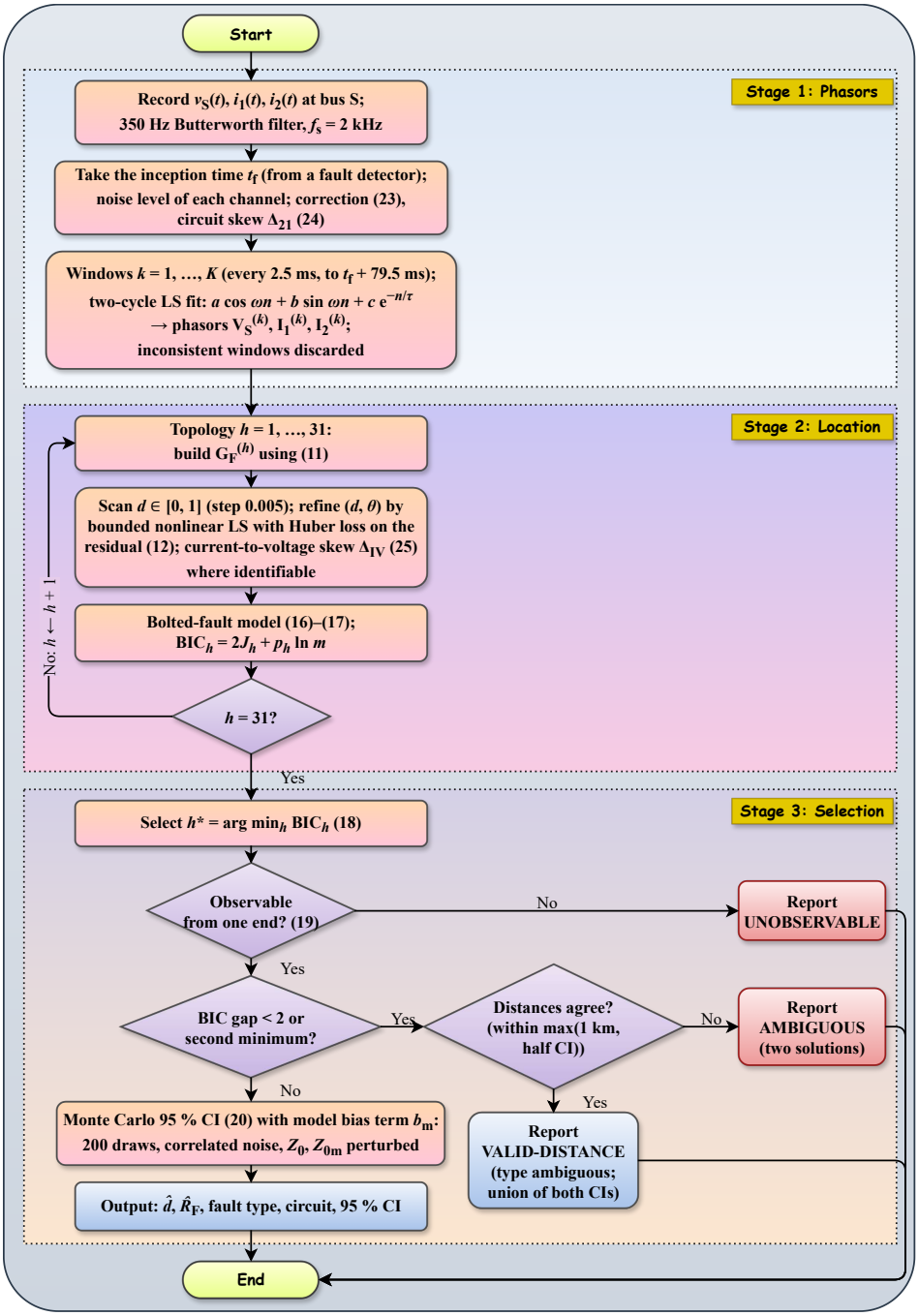


Fig. 2 Flowchart of the proposed method

Algorithm 1 Proposed fault location method

Step	Operation
1	**Input:** line data $\mathbf{Z}'$, $\mathbf{Y}'$, ℓ; sampled $v_S(t)$, $i_1(t)$, $i_2(t)$ at bus S;
2	Take the inception time t_f (from a fault detector); estimate the noise level of each channel from the last prefault cycle; optionally correct each channel by its certificate factor k_{ch} (23); estimate the circuit-to-circuit skew Δ_{21} from the prefault state (24);
3	**for** k = 1 : K (two-cycle windows every 2.5 ms, the last ending at t_f + 79.5 ms); discard windows inconsistent with their neighbours
4	Estimate the phasors $\mathbf{x}_S^{(k)}$ by the least-squares fit (5)–(7);
5	**end for**
6	**for** h = 1 : 31 (fault types, Table 1)
7	Build $\mathbf{G}_F^{(h)}$ using (11);
8	Scan d $\in$ [0, 1] with a step of 0.005; for each d, obtain the conductances θ and the residual (12) using (8)–(12);
9	Refine (d, θ) at the best minima by minimising (15); estimate the current-to-voltage skew Δ_{IV} jointly where it is identifiable (25);
10	Fit the bolted-fault model (16) and accept it if (17) holds;
11	Calculate J_h and BIC_h using (18);
12	**end for**
13	Select $h^* = \arg\min_h \mathrm{BIC}_h$;
	Observability and uniqueness check:
14a	**if** (19) holds, **report** UNOBSERVABLE; go to step 16;
14b	**if** $\mathrm{BIC}_{(2)} - \mathrm{BIC}_{(1)} < 2$, or a second minimum of J_{h^*} lies within 10 % of its cost and at least 0.05 p.u. away: calculate the intervals (20) of both solutions; **if** their distances agree within max(1 km, half the interval width), **report** VALID-DISTANCE; **else report** AMBIGUOUS with both solutions; go to step 16;
15	Calculate the 95 % confidence interval of d using (20) with the model bias term;
16	**Output:** $\hat{d}$, $\hat{R}_F$, fault type, faulted circuit and confidence interval.

where T_s is the sampling interval, a and b are the quadrature components of the fundamental, c and τ are the initial value and time constant of the decaying component, and $\varepsilon[\mathrm{n}]$ is the measurement noise. For a fixed τ, (5) is linear in $\boldsymbol{\beta} = [a\ b\ c]^{\mathsf{T}}$, which is obtained by least squares:

$$\hat{\boldsymbol{\beta}}(\tau) = \left(\boldsymbol{\Phi}_\tau^{\mathsf{T}}\boldsymbol{\Phi}_\tau\right)^{-1}\boldsymbol{\Phi}_\tau^{\mathsf{T}}\mathbf{x}, \qquad \hat{\tau} = \arg\min_{\tau\in[2\ \mathrm{ms},\,5\ \mathrm{s}]} \left\|\mathbf{x} - \boldsymbol{\Phi}_\tau\hat{\boldsymbol{\beta}}(\tau)\right\|^2 \tag{6}$$

where $\boldsymbol{\Phi}_\tau$ is the 2N×3 regressor matrix with rows $[\cos(\omega n T_s)\ \ \sin(\omega n T_s)\ \ e^{-nT_s/\tau}]$. The one-dimensional search over τ is performed by bounded scalar minimisation. The phasor of the channel is

$$\hat{X} = \frac{\hat{a} - j\hat{b}}{\sqrt{2}\,H(j\omega)} \tag{7}$$

where $H(j\omega)$ is the 50 Hz response of the fourth-order Butterworth antialiasing filter (cutoff 350 Hz). Compared with the one-cycle DFT, (5)–(7) reduce the phasor error for bolted faults from $5.8{\times}10^{-2}$ to about $4{\times}10^{-5}$.

The first postfault cycles also contain lightly damped natural oscillations of the line (about 330, 390 and 590 Hz for the studied line, with decay times of 30–96 ms), which the antialiasing filter attenuates only partly. Therefore, K two-cycle windows shifted by 5 samples (2.5 ms) are used. The first window starts at t_f + 27 ms (one cycle plus the 7 ms filter settling time) and the last ends 79.5 ms after inception, so that K = 6. Windows whose phasors differ from those of their neighbours by more than 0.5 % in magnitude or 0.5° in angle on any channel are discarded, with at least three windows retained. The residuals of all retained windows are combined into one estimation problem in Stage 2.

2.4 Stage 2: Common-bus formulation and estimation for each topology

As shown in Fig. 1b, let a fault occur at the per-unit distance d ∈ [0, 1] from bus S. The state just before the fault point F is obtained from the sending-end phasors of window k by (3):

$$\mathbf{x}(F^-) = \mathbf{T}(d\ell)\,\mathbf{x}_S^{(k)}, \qquad \mathbf{V}_F = \mathbf{V}(F^-) \tag{8}$$

At the fault point, the voltages are continuous and the currents are reduced by the fault current vector $\mathbf{I}_F \in \mathbb{C}^6$:

$$\mathbf{x}(F^+) = \mathbf{x}(F^-) - \begin{bmatrix}\mathbf{0}\\ \mathbf{I}_F\end{bmatrix}, \qquad \mathbf{x}_R = \mathbf{T}\big((1-d)\ell\big)\,\mathbf{x}(F^+) \tag{9}$$

where $\mathbf{x}_R = [\mathbf{V}_R;\ \mathbf{I}_R]$ is the state at bus R. The remote source and its impedance are unknown to a single-ended locator. However, both circuits terminate at bus R, so the receiving-end voltages calculated through circuit 1 and circuit 2 must be equal, independent of the remote network:

$$\mathbf{V}_{R,1:3}(d,\boldsymbol{\theta}) - \mathbf{V}_{R,4:6}(d,\boldsymbol{\theta}) = \mathbf{0} \tag{10}$$

Equation (10) gives three complex (six real) equations per window that contain no remote-end quantity, which makes the problem solvable from one end.

A resistive fault is represented by branch conductances $g_{p,i} \geq 0$ from each faulted conductor i to a common fault node and a conductance $g_g \geq 0$ from this node to ground. Elimination of the common node gives

$$\mathbf{I}_F = \mathbf{G}_F(\boldsymbol{\theta})\,\mathbf{V}_F, \qquad \mathbf{G}_F = \operatorname{diag}(\mathbf{g}_p) - \frac{\mathbf{g}_p\mathbf{g}_p^{\mathsf{T}}}{\mathbf{1}^{\mathsf{T}}\mathbf{g}_p + g_g} \tag{11}$$

where $\mathbf{g}_p \in \mathbb{R}^6$ contains the branch conductances (zero for healthy conductors), $\boldsymbol{\theta} = (\mathbf{g}_p, g_g)$ and $\mathbf{1}$ is a vector of ones; an ungrounded fault has $g_g = 0$. Each combination of faulted conductors and ground connection defines a topology h. The method considers the 31 topologies of Table 1: all single-circuit faults, the ungrounded cross-circuit faults between different phases and the grounded cross-circuit faults between

the same phases, which are the most frequent intercircuit faults on double-circuit towers. Faults that involve more conductors of both circuits (e.g. A1B1C2) are not included and are fitted by the closest fault type with a larger residual. Substituting (8), (9) and (11) into (10) gives the residual of window k:

$$\mathbf{r}^{(k)}(d,\boldsymbol{\theta}) = \mathbf{E}\,\mathbf{T}\big((1-d)\ell\big)\left(\mathbf{I}_{12} - \begin{bmatrix} \mathbf{0} & \mathbf{0} \\ \mathbf{G}_F(\boldsymbol{\theta}) & \mathbf{0} \end{bmatrix}\right)\mathbf{T}(d\ell)\,\mathbf{x}_S^{(k)}, \qquad \mathbf{E} = [\,\mathbf{I}_3 \quad -\mathbf{I}_3 \quad \mathbf{0}_{3\times 6}\,] \tag{12}$$

where $\mathbf{I}_n$ is the n×n identity matrix. The real and imaginary parts of the entries of $\mathbf{r}^{(k)}$, k = 1, …, K, are denoted $r_{q,k}$ and normalised by their standard deviations:

$$\tilde{r}_{q,k} = \frac{r_{q,k}(d,\boldsymbol{\theta})}{\sigma_{q,k}}, \qquad \sigma_{q,k}^2 = \sigma_{\text{noise},q,k}^2 + \sigma_{\text{param},q,k}^2 + \sigma_{\text{fit},q,k}^2 \tag{13}$$

where σ_{noise} is the measurement noise propagated from the prefault noise estimate of each channel, σ_{param} is the contribution of a 5 % (one standard deviation) uncertainty of Z_0 and Z_{0m}, and σ_{fit} is the postfault residual of the phasor fit (6), which accounts for model errors not explained by noise. The normalised residuals are weighted by the Huber function [58]

$$\rho_\delta(u) = \begin{cases} \tfrac{1}{2}u^2, & |u| \le \delta \\ \delta|u| - \tfrac{1}{2}\delta^2, & |u| > \delta \end{cases}, \qquad \delta = 1.345 \tag{14}$$

which is quadratic for small and linear for large residuals, so that a single corrupted channel or window cannot dominate the estimate. For topology h, the estimate is

$$(\hat{d},\hat{\boldsymbol{\theta}})_h = \arg\min_{0\le d\le 1,\ \boldsymbol{\theta}\ge\mathbf{0}} J_h(d,\boldsymbol{\theta}), \qquad J_h = \sum_{k=1}^{K}\sum_{q}\rho_\delta(\tilde{r}_{q,k}) \tag{15}$$

Problem (15) is solved globally in d and locally in θ. The distance is first scanned over [0, 1] with a step of 0.005 (1.25 km for ℓ = 250 km), with θ optimised at each step, and the best minima are then refined jointly by a bounded trust-region least-squares solver. Thus, no fixed-point distance update is used; only the local refinement is iterative, and a non-converged refinement is reported.

The phase branches of a topology share one conductance, and a grounded topology has one additional ground conductance. For the cross-circuit same-phase-to-ground topologies, the two phase branches are fixed at a contact resistance of 1 Ω, so that only the ground conductance is free. The number of free parameters p_h of topology h, including the distance, is therefore at most 3 (Table 1). All simulated faults have equal branch resistances; faults with unequal branch resistances were not tested. After the fit, a topology is excluded if one of its faulted branches carries less than 5 % of the largest branch current, because such a branch is not supported by the data.

As $R_F \to 0$, the voltages of the faulted conductors at F tend to zero (about 20 V for a phase voltage of 290 kV in the studied cases), the conductances in (11) become very large, and a fault on the other circuit at a different distance may satisfy (10) almost equally well. Therefore, a bolted-fault model is also fitted for each topology:

Table 1 Fault types considered by the proposed method

Group	Members	Number	p
Single-circuit phase-to-ground	A1G, B1G, C1G, A2G, B2G, C2G	6	2
Single-circuit phase-to-phase	A1B1, B1C1, A1C1, A2B2, B2C2, A2C2	6	2
Single-circuit phase-to-phase-to-ground	A1B1G, B1C1G, A1C1G, A2B2G, B2C2G, A2C2G	6	3
Single-circuit three-phase	A1B1C1, A2B2C2	2	2
Single-circuit three-phase-to-ground	A1B1C1G, A2B2C2G	2	3
Cross-circuit, different phases, ungrounded	A1B2, A1C2, B1A2, B1C2, C1A2, C1B2	6	2
Cross-circuit, same phase, to ground	A1A2G, B1B2G, C1C2G	3	2
Total		31	

p: number of free parameters (distance and conductances).

$$V_{F,i} = 0 \quad \text{for every faulted conductor } i, \qquad \mathbf{I}_F \text{ free} \tag{16}$$

The bolted solution is accepted only if the root-mean-square value of its unweighted residual, relative to the nominal phase voltage, satisfies

$$\frac{1}{V_n}\sqrt{J_h^{\mathrm{b}}/m} \le \max\left(\epsilon_b,\ \kappa\,\sigma_{\mathrm{floor}}\right), \qquad \epsilon_b = 6.8\times10^{-3},\ \kappa = 5 \tag{17}$$

where J_h^{b} is the unweighted sum of squared residuals of (10) and (16), m is the number of real residuals, V_n is the nominal phase voltage and σ_{floor} is the noise floor propagated through the residual operator of the bolted model. An accepted bolted fit replaces the resistive fit only if its residual is also lower, and it is counted in (18) with the parameter number p_h of its topology. The threshold ϵ_b is the geometric mean of the largest residual of a bolted fault (1.15×10^{-3}) and the smallest residual of a resistive fault (4.06×10^{-2}, $R_F = 5\ \Omega$) in a separate tuning set (Section 3); in all test sets, resistive faults gave residuals of at least 0.137. A lower threshold of 10^{-3} would reject bolted faults with residuals of 1.0–1.8×10^{-3}; two such faults were then located on the parallel circuit with errors of 13.4 % and 46.7 %.

2.5 Stage 3: Topology selection, observability and confidence interval

The topology is selected by the BIC [56], which penalises the number of parameters so that a topology with more faulted conductors is not preferred only because of its additional freedom:

$$\mathrm{BIC}_h = 2J_h + p_h \ln m, \qquad h^* = \arg\min_h \mathrm{BIC}_h \tag{18}$$

Since the residuals are normalised by their standard deviations (13), $2J_h$ equals, up to a constant, minus twice the log-likelihood of the least-favourable (Huber) error distribution associated with (14) [54], and it reduces to the Gaussian case for residuals within $\pm\delta$; (18) is therefore the BIC of a robust quasi-likelihood. Because the windows overlap, the m residuals are not independent and the penalty $p_h \ln m$ is conservative; as all fault types are evaluated on the same windows, this affects the selection only

through the size of the penalty. The result is considered ambiguous if the two smallest values of (18) differ by less than 2, or if the cost function of the selected topology has a second local minimum within 10 % of its cost and at least 0.05 p.u. away. In this case, the confidence intervals (20) of the two best solutions are calculated. On a double-circuit line, both circuits share the towers, so the distance is more important for the line inspection than the circuit. Therefore, if the two distances agree within max(1 km, half the interval width), the distance is reported as valid with the label VALID-DISTANCE (type or circuit ambiguous) and the union of both intervals; otherwise, the result is reported as AMBIGUOUS with both solutions.

A fault between the same phases of both circuits to ground (e.g. A1A2G) cannot be located from one end: because of the symmetry of the line, a family of distances and conductances satisfies (10) almost equally well. This is detected from the Jacobian $\mathbf{J}_{d\theta}$ of the normalised residuals with respect to (d, θ):

$$\sigma_{\min}(\mathbf{J}_{d\theta}) < \eta \tag{19}$$

where $\sigma_{\min}$ is the smallest singular value of the Jacobian with columns scaled to relative sensitivities and $\eta = 10^{-6}\sigma_{\max}$. A fault is also reported as UNOBSERVABLE if the healthy-line model explains the circuit difference almost as well as the best topology (BIC difference below 10). In both cases, no distance is returned.

These properties follow from the structure of (10). Each window provides six real equations, and since overlapping windows are strongly correlated, the effective number of independent equations is close to six, against at most three free parameters. With independent branch conductances, a three-phase-to-ground fault would have five unknowns, which explains why its ground connection cannot be identified from terminal data. Moreover, (10) depends only on the difference between the two circuits. For identical circuits, whose chain matrix commutes with the exchange of the circuits, a fault current that is identical in both circuits lies in the null space of $\mathbf{E}$ in (12). Hence, every grounded circuit-symmetric fault (A1A2G, A1B1A2B2G, ...) is unobservable from (10), and an ungrounded A1A2 fault is practically unobservable because the voltages of the two faulted conductors are almost equal. For nonidentical circuits, these faults may become weakly observable; the observability test detects all of them. For the single-loop faults (phase-to-ground, phase-to-phase and three-phase), a current-to-voltage time skew or a fault reactance changes the fault loop angle in the same way as a change of d, whereas the additional ground loop of a phase-to-phase-to-ground fault makes the skew identifiable (Section 4.1.1). If the remote source data are known, an optional source-assisted mode adds the bus-R Thévenin condition $\mathbf{V}_{R,1:3} - \mathbf{Z}_R(\mathbf{I}_{R,1:3} + \mathbf{I}_{R,4:6}) = \mathbf{E}_R$, with the remote source voltage $\mathbf{E}_R$ and impedance $\mathbf{Z}_R$, to (10) and locates such faults; its results are reported separately.

Finally, the 95 % confidence interval of d is obtained by Monte Carlo propagation [51] with B = 200 draws. In each draw b, sample-level noise with the estimated level is added to the recorded signals and processed with the same overlapping windows, so that the noise is correlated across windows as in the measured data, and Z_0 and Z_{0m} are perturbed with a standard deviation of 5 %. The distance $\hat{d}^{(b)}$ is re-estimated locally, and

$$\mathrm{CI}_{95} = \left[Q_{0.025}\{\hat{d}^{(b)}\},\ Q_{0.975}\{\hat{d}^{(b)}\} \right] \tag{20}$$

where Q_p is the empirical p-quantile over the B draws. The draws contain noise and parameter uncertainty but not the deterministic difference between the plant and the model, which dominates for bolted and ungrounded faults, whose intervals would otherwise be only a few metres wide. Therefore, each side of (20) is widened in quadrature by a model bias term b_m: $[\hat{d}\ell - (w_-^2 + b_m^2)^{1/2},\ \hat{d}\ell + (w_+^2 + b_m^2)^{1/2}]$, where $w_{\mp}$ are the distances from $\hat{d}\ell$ to the quantiles of (20) and $b_m = 0.074$ km $\times$ $\ell/250$ km is the 95th percentile of the location error in the tuning set. The interval is conditional on the selected topology, except for VALID-DISTANCE results, for which the union over both solutions is used. A result is labelled VALID if neither (19) nor the ambiguity condition holds and the refinement converges. The parameters of the method are listed in Table 2.

Table 2 Parameters of the proposed method

Quantity	**Value**
Recorder	4th-order Butterworth, 350 Hz; $f_s = 2$ kHz; settling time 7 ms
Phasor fit	two cycles; $\tau \in [2$ ms, 5 s]
Data windows	shift 2.5 ms; first start $t_f + 27$ ms; last end $t_f + 79.5$ ms (K = 6)
Window consistency	< 0.5 % in magnitude and $< 0.5^\circ$ in angle; at least 3 windows
σ_{noise}	rms residual of a sine fit to the last prefault cycle (floor 10^{-6} of the magnitude)
σ_{param}	5 % (one standard deviation) on Z_0 and Z_{0m}
σ_{fit}	rms residual of the postfault phasor fit (6)
Distance scan / refinement	step 0.005 p.u. / tolerance 10^{-5} p.u.
Huber constant δ	1.345
Branch current threshold	5 % of the largest branch current
Ambiguity	BIC difference < 2; second minimum within 10 % and ≥ 0.05 p.u. away
Observability	$\sigma_{\min} < 10^{-6}\ \sigma_{\max}$; healthy-model BIC difference < 10
Bolted-fault model (17)	$\epsilon_b = 6.8{\times}10^{-3}$, $\kappa = 5$
Distance agreement	max(1 km, half the interval width)
Confidence interval	B = 200; $b_m = 0.074$ km $\times$ $\ell/250$ km
Skew estimation (24), (25)	$\lvert\Delta\rvert \leq 300$ μs (≤ 25 μs after (23)); grid 50 μs

3 Simulation results

The proposed method was tested on the 500 kV, 50 Hz, 250 km double-circuit line shown in Fig. 3. The line connects two Thévenin equivalents at buses S and R, and the fault locator is installed at bus S. The line and source parameters are listed in Table 3 [33]; the source impedances correspond to the 500 kV level (scaling factor $(500/400)^2 = 1.5625$). The two circuits are identical and transposed in the base case; untransposed and nonidentical circuits are considered in Section 3.4.

The main study comprises 990 cases (Table 4): five fault types, eleven fault distances, three inception angles and six fault resistances. The fault resistance R_F is defined for each fault type as given in Table 5, and the ungrounded faults with $R_F =$

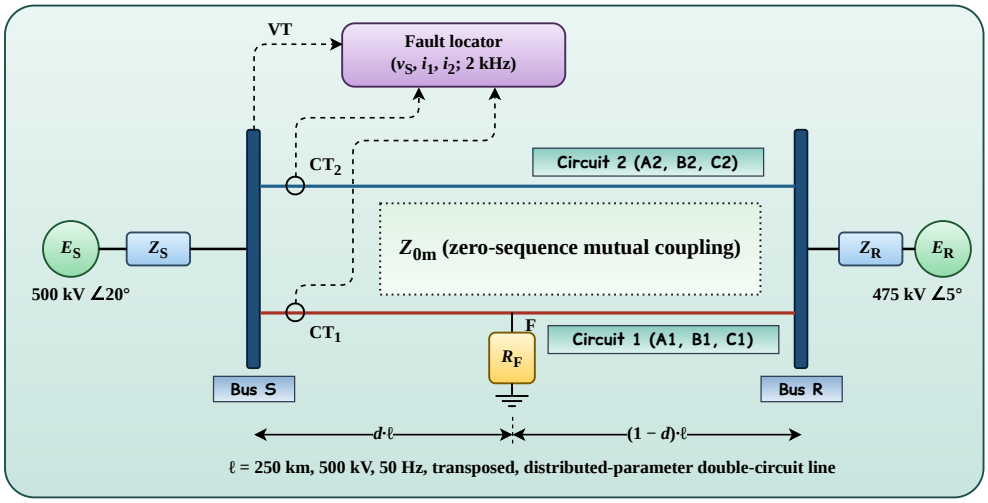


Fig. 3 Single-line diagram of the 500 kV double-circuit test system

Table 3 Parameters of the test system

Quantity	Value
Nominal voltage, frequency, length	500 kV, 50 Hz, ℓ = 250 km (150–400 km in the line length study)
Positive-sequence R_1, X_1, C_1 (per km)	0.0268 Ω, 0.3139 Ω, 11.662 nF
Zero-sequence R_0, X_0, C_0 (per km)	0.2102 Ω, 1.1651 Ω, 6.996 nF
Zero-sequence mutual R_{0m}, X_{0m}, C_{0m} (per km)	0.1834 Ω, 0.7621 Ω, −2.1088 nF[a]
Source S: E_S; Z_1; Z_0	500 kV ∠20°; 0.50 + j8.50 Ω; 1.25 + j7.00 Ω
Source R: E_R; Z_1; Z_0	475 kV ∠5°; 0.75 + j13.00 Ω; 5.75 + j20.50 Ω
Recorder	4th-order Butterworth, 350 Hz; f_s = 2 kHz (N = 40 samples per cycle)

[a] Intercircuit entry of the nodal capacitance matrix ($C_{0m}/3$), negative by definition.

80–320 Ω form a separate high-resistance group. Four additional case sets were used to test generalisation (Table 4): prefault loading (load angles $\delta = 5°$ and 30°; 286 cases), line length (150, 200, 300 and 400 km; 352 cases), unseen cases (30 cases whose parameter values occur in no other set) and a high-fidelity set (13 cases simulated in Simscape Electrical with a finer line model). The thresholds ϵ_b and b_m and the skew identifiability threshold were determined on a separate tuning set of 128 cases (Table 4) and eight inductive fault cases; no test case was used for this purpose. The noise study, the comparison of phasor estimators, the ablation, the ±10 % R, Z_{0m} and C cases of the parameter study, the gain error cases and the CT saturation and combined error tests were performed with $\epsilon_b = 10^{-3}$, without the model bias term and without the distance agreement rule. The fault inception time t_f was assumed to be known.

Table 4 Simulated case sets

Set	Fault types	R_F (Ω)	d (p.u.)	Inception angle	Cases
Main, grounded	AG, BCG, A1A2G	0.001, 20, 40, 80, 160, 320	0.05, 0.1, 0.2, …, 0.9, 0.95	0°, 45°, 90°	594
Main, ungrounded	BC, ABC	0.001, 20, 40	as above	as above	198
Main, high resistance	BC, ABC	80, 160, 320	as above	as above	198
Loading ($\delta = 5°$, 30°)	all five	AG, BCG, A1A2G: 0.001, 80, 320; BC, ABC: 0.001, 40	as above	0°	286
Line length (150, 200, 300, 400 km)	AG, BC, A1A2G	AG, A1A2G: 0.001, 80, 320; BC: 0.001, 40	as above	0°	352
Unseen	all five	55, 230	0.37, 0.63, 0.88	30°	30
High fidelity (Simscape, 50 + 50 π-sections)	AG, BCG, A1A2G; BC	20, 320; BC: 0.001	0.5, 0.95; BC: 0.5	0°	13
Tuning (not used for testing)	AG, BC, BCG, ABC	0.001, 5, 60, 250	0.15, 0.45, 0.75, 0.92	20°, 70°	128

Table 5 Definition of the fault resistance R_F

Fault	Meaning of R_F	Branch per faulted conductor	Ground branch
AG	phase-to-ground resistance	0.001 Ω	R_F
BC	phase-to-phase resistance	$R_F/2$	open
BCG	phase-to-ground resistance of each phase	R_F	0.001 Ω
ABC	phase-to-phase resistance	$R_F/2$	open
A1A2G	ground path resistance, conductors in contact	1 Ω	R_F

The test system is a six-conductor network with 25 coupled π-sections on each side of the fault (more for lines longer than 250 km, so that no section exceeds 10 km), the two sources and the fault branches. It was first modelled in MATLAB/Simscape Electrical R2026a, where each case required 685–1849 s, mainly to simulate the 1 s prefault interval of a stiff network with 606 states. Since the network is linear and switches only once, the cases were computed by an exact state-space solution of the same network: the prefault steady state is solved in the phasor domain, and the postfault state is the postfault steady state plus a transient obtained by the matrix exponential,

$$\mathbf{x}(t) = \mathbf{x}_{p,\mathrm{post}}(t) + e^{\mathbf{A}_{\mathrm{post}}(t-t_f)}\left(\mathbf{x}_{p,\mathrm{pre}}(t_f) - \mathbf{x}_{p,\mathrm{post}}(t_f)\right) \tag{21}$$

where $\mathbf{A}_{\mathrm{post}}$ is the state matrix of the faulted network and $\mathbf{x}_{p,\mathrm{pre}}$, $\mathbf{x}_{p,\mathrm{post}}$ are the prefault and postfault steady-state solutions. Equation (21) has no time discretisation error and required about 6 s per case. Fig. 4 compares the waveforms obtained by (21) and by Simscape; from 10 ms before to 60 ms after inception, the phase-A current of circuit 1 differs by at most 0.03 A on a peak of 1287 A. For nine cases simulated with both tools, the phasors agreed within 4.6×10^{-7} (relative) and the estimated locations within 6 mm. The estimator always uses the distributed-parameter model

(3), whereas the plant consists of lumped π-sections and all signals pass through the recorder model; the estimator model therefore differs from the plant, although both use the same per-unit-length parameters.

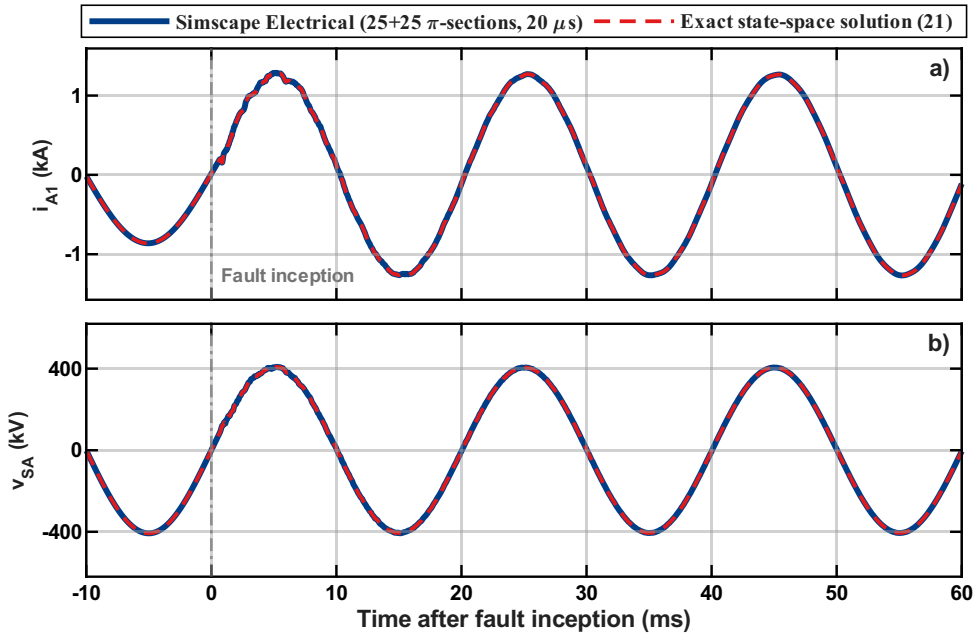


Fig. 4 a) Current and b) voltage of phase A at bus S: Simscape and state-space solution (21)

The proposed method is compared with the single-ended method of Khodadadi Arpanahi et al. [33], which was implemented and verified on its original test system (Sections 3.2 and 3.4). Its phase-to-phase distance update (Eq. (21) of [33]) uses the fault-point voltage of the previous iteration and did not always converge; therefore, a rearranged form of the same update with the same fixed point is used, which converges in 1–5 iterations (Appendix A). Results of the original update are also reported where relevant. Both methods process the same recorded signals. The method of [33] uses one-cycle DFT phasors of the first window starting 27 ms after inception, and the actual fault type is supplied to it, which can only favour it. The fault location error is defined as

$$\mathrm{FLE} = \frac{|\hat{x}_F - x_F|}{\ell} \times 100\ \% = |\hat{d} - d| \times 100\ \% \tag{22}$$

where x_F and $\hat{x}_F$ are the actual and estimated fault distances in km. The proposed method returns a valid location or one of the labels AMBIGUOUS and UNOBSERVABLE; the method of [33] returns a distance whenever its iteration converges within the line. A result of the proposed method is called type identified if it is valid with a unique topology, and distance valid if it is type identified or VALID-DISTANCE. FLE statistics are calculated over the valid results, and two rates are reported: the share

of valid results and the share of all cases located with FLE < 1 %, which counts a wrong and a missing distance equally as a failure. Unless stated otherwise, the statistics refer to the four fault types that are observable from one end (AG, BCG, BC and ABC), and A1A2G faults are reported separately. Paired comparisons use the Wilcoxon signed-rank test, and 95th percentiles are calculated as in the MATLAB prctile function.

The two methods also use different data lengths. The method of [33] uses one cycle of postfault data and gives a result about 47 ms after inception, whereas the proposed method uses data up to 79.5 ms after inception and then requires a few seconds of computation (Section 3.3). This is acceptable because fault location is performed after fault clearing. However, the record must not contain a breaker operation; if the faulted circuit is opened earlier, (10) no longer holds, and the number of windows K must be limited to the part of the record before the first breaker operation.

3.1 Effect of fault type, location and resistance

Figs. 5, 6, 7 and 8 show the estimated fault location of both methods versus the fault resistance (R_F = 0.001, 20, 40, 80, 160 and 320 Ω) for ten fault locations between d = 0.1 and 0.95 p.u. for AG, BCG, BC and ABC faults, respectively.

For all fault resistances, the estimates of the proposed method coincide with the actual locations within the resolution of the plots. Over the 60 cases per fault type (0° inception), the maximum deviation $|\hat{d} - d|$ of the proposed method is 4.5×10^{-4}, 9.3×10^{-4}, 3.1×10^{-4} and 1.4×10^{-4} p.u. for AG, BCG, BC and ABC faults, compared with 6.6×10^{-2}, 1.6×10^{-2}, 1.0×10^{-2} and 6.4×10^{-2} p.u. for the method of [33]. The method of [33] underestimates the fault distance. For bolted AG faults, its deviation increases with the distance (0.471 p.u. for d = 0.5 and 0.838 p.u. for d = 0.9), and for R_F = 20–320 Ω its estimates lie up to about 0.016 p.u. below the actual location. The FLE of the proposed method is shown in Fig. 9, and the statistics of both methods are given in Table 6.

Table 6 FLE (%) by fault type, main study

		Proposed method					Method of [33]				
Fault type	**Cases**	**Valid**	**Mean**	**Median**	**95th**	**<1 %**	**Valid**	**Mean**	**Median**	**95th**	**<1 %**
AG	198	100.0	0.0085	0.0033	0.039	100.0	100.0	0.659	0.298	2.25	77.8
BCG	198	100.0	0.0056	0.0021	0.021	100.0	100.0	0.592	0.331	1.61	80.8
BC	198	98.5	0.0036	0.0012	0.014	98.5	100.0	0.537	0.220	2.60	90.9
ABC	198	99.5	0.0020	0.0007	0.0095	99.5	100.0	0.739	0.285	4.24	86.4
All	792	99.5	0.0049	0.0014	0.022	99.5	100.0	0.632	0.270	2.92	84.0
A1A2G	198	0*	–	–	–	0	37.4	24.5	20.0	67.8	3.0

Valid and <1 %: share of cases (%) with a valid result and with FLE < 1 %. * All 198 cases reported as UNOBSERVABLE; the method of [33] returned a distance in 74 cases, 68 of them with FLE > 1 %.

According to Table 6, the median FLE of the proposed method is 0.0007–0.0033 % (1.8–8.3 m) for the four observable fault types, against 0.220–0.331 % (550–830 m)

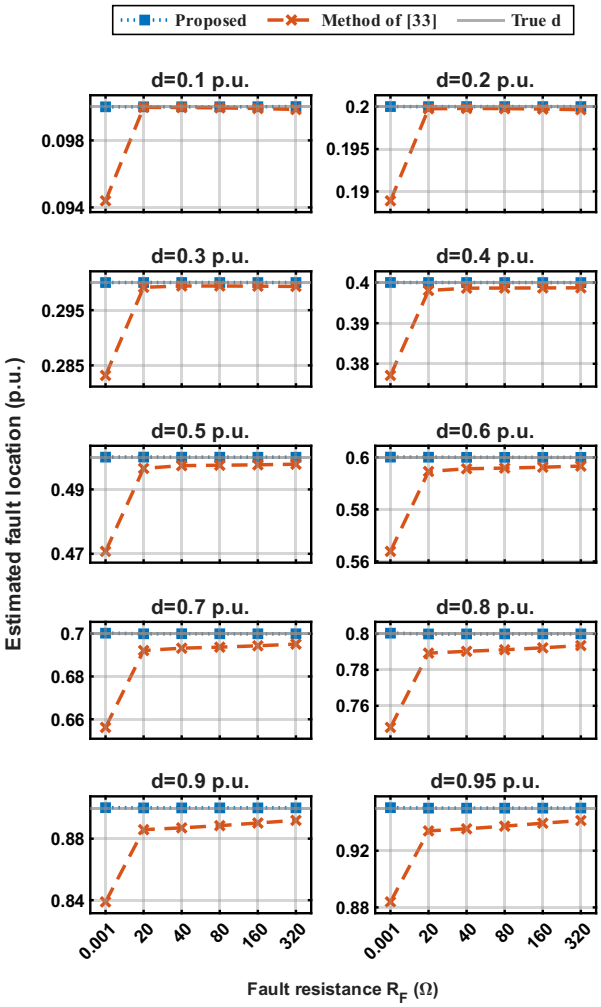


Fig. 5 Estimated fault location versus fault resistance, AG faults

for the method of [33]. For BC faults, the original update did not converge in 94.9 % of the cases, whereas the rearranged update converged in all of them. For bolted faults, the voltages of the faulted conductors at the fault point are almost zero, so a cross-circuit topology at another distance can reproduce the measured phasors nearly as well as the actual fault; with the bolted-fault model (16)–(17), all 308 bolted faults of observable types in the four test sets are located. Among the 1243 type-identified locations of observable faults in all 1658 cases, the maximum FLE is 0.28 % (AG fault at d = 0.95, R_F = 320 Ω, 400 km line) and the 99th percentile is 0.067 %; the ten VALID-DISTANCE results have a maximum FLE of 0.063 %. All 198 A1A2G faults were reported as UNOBSERVABLE, as expected from Section 2.5, whereas the method of [33] returned a distance in 37.4 % of them with a mean FLE of 24.5 % and without any indication of the error. With the remote source impedance known, the

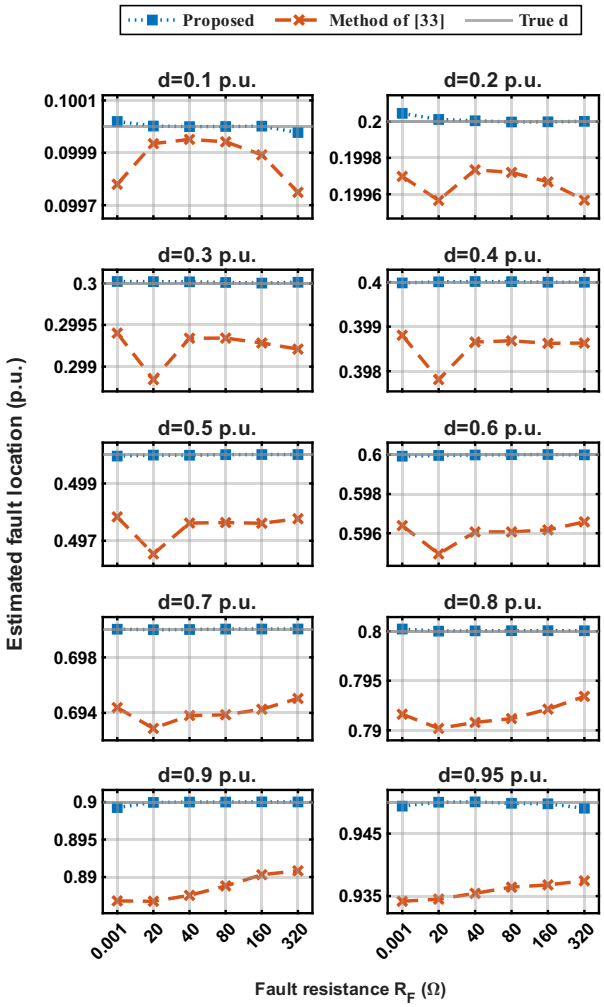


Fig. 6 Estimated fault location versus fault resistance, BCG faults

source-assisted mode located these faults with a mean FLE of 0.0087 %. The share of valid results alone does not describe the accuracy: for the 792 observable cases, the method of [33] returns a distance in all cases but locates only 84.0 % within 1 %, against 99.5 % for the proposed method. The remaining four observable cases are not located wrongly: three BC faults with $R_F = 320\ \Omega$ and 90° inception are reported as UNOBSERVABLE because their contribution to the circuit difference is too small, and one ABC fault is reported as VALID-DISTANCE.

Fig. 9 also shows the dependence of the FLE on the fault location. For the method of [33], the mean FLE of AG faults increases from 0.028 % at d = 0.05 to 1.86 % at d = 0.95, which is the expected effect of the remote infeed through the fault resistance. The FLE of the proposed method also increases towards the remote end but remains below 0.05 % at every location. At 0° inception, its maximum FLE is 0.045 %, 0.093

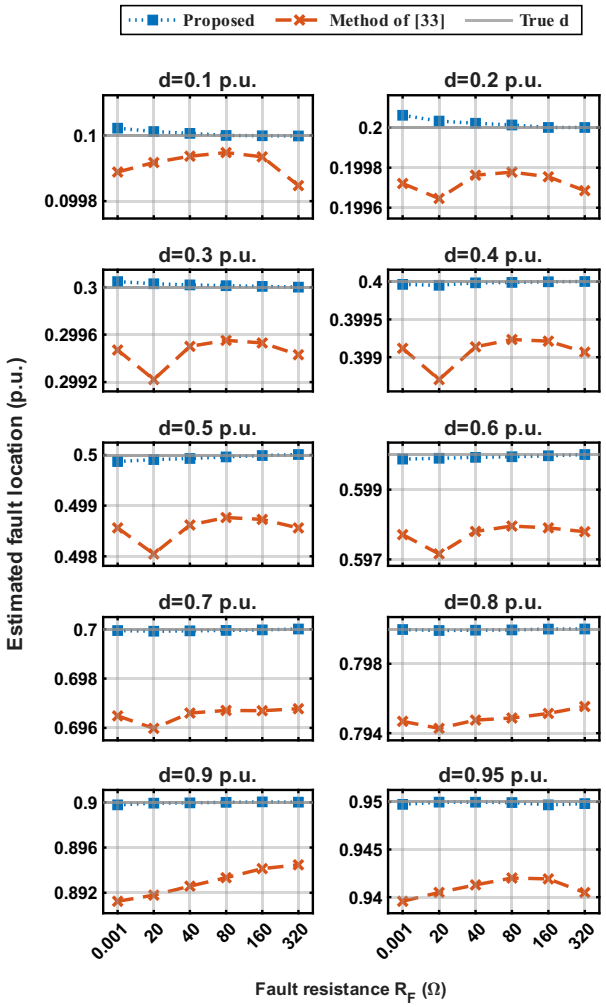


Fig. 7 Estimated fault location versus fault resistance, BC faults

%, 0.031 % and 0.014 % for AG, BCG, BC and ABC faults, against 6.61 %, 1.58 %, 1.04 % and 6.43 % for the method of [33]; for d $<$ 0.5, the maxima of the proposed method do not exceed 0.0062 %, whereas those of the method of [33] reach 2.47 %.

Table 7 gives the effect of the fault resistance. For 20–320 Ω, the median FLE of the proposed method is 0.0009–0.0024 % and its 95th percentile does not exceed 0.034 %, whereas the median FLE of the method of [33] is 0.171–0.322 %. Bolted faults are the most difficult case for both methods; nevertheless, the median FLE of the proposed method for bolted faults (0.0034 %) is about 385 times lower than that of the method of [33] (1.31 %), and all bolted faults are located within 1 % (maximum 0.074 %), compared with 40.9 % for the method of [33]. The share of valid results is 97.7–100 % for every fault resistance, and the remaining cases are reported as UNOBSERVABLE or VALID-DISTANCE rather than located wrongly.

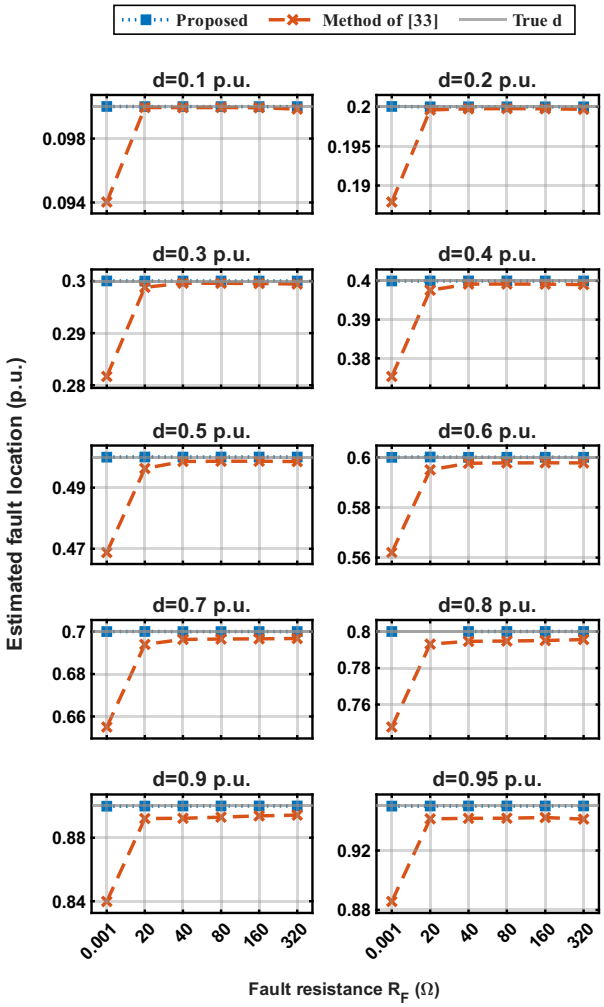


Fig. 8 Estimated fault location versus fault resistance, ABC faults

Table 7 FLE (%) versus fault resistance, main study, observable fault types

		Proposed method					Method of [33]				
R_F (Ω)	Cases	Valid	Mean	Median	95th	<1 %	Valid	Mean	Median	95th	<1 %
0.001	132	100.0	0.0092	0.0034	0.045	100.0	100.0	2.01	1.31	5.99	40.9
20	132	99.2	0.0042	0.0024	0.017	99.2	100.0	0.442	0.322	1.41	88.6
40	132	100.0	0.0029	0.0013	0.011	100.0	100.0	0.368	0.183	1.29	90.9
80	132	100.0	0.0035	0.0010	0.014	100.0	100.0	0.347	0.175	1.15	90.9
160	132	100.0	0.0037	0.0009	0.017	100.0	100.0	0.322	0.178	0.976	95.5
320	132	97.7	0.0060	0.0012	0.034	97.7	100.0	0.303	0.171	0.903	97.0

Columns as in Table 6.

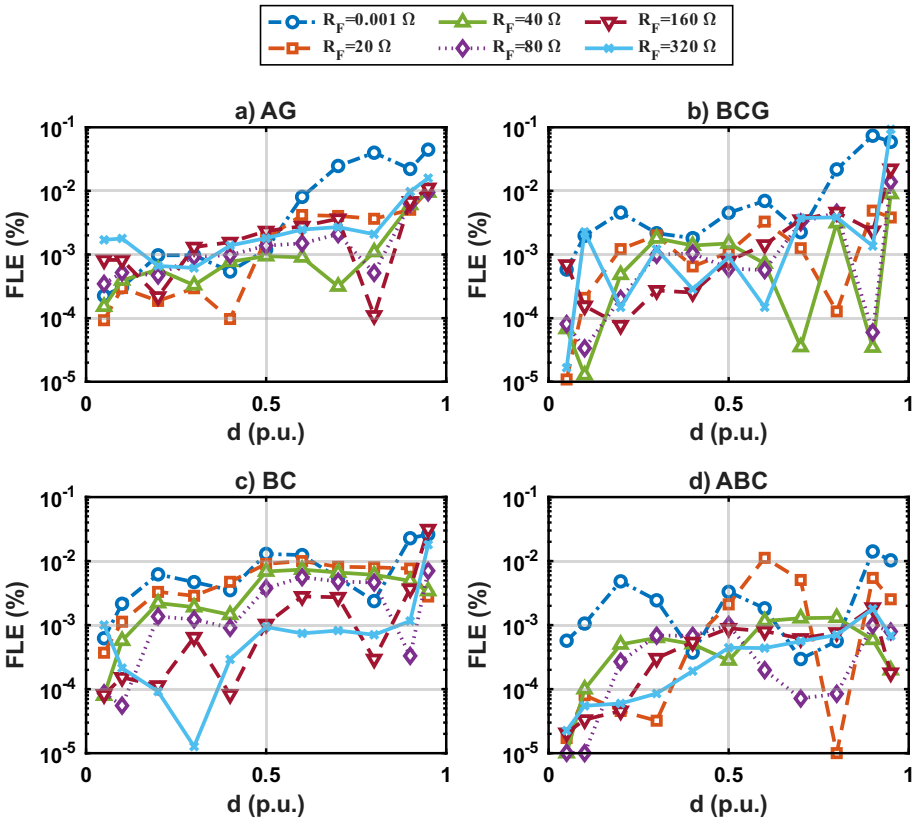


Fig. 9 FLE of the proposed method versus fault location: a) AG, b) BCG, c) BC and d) ABC faults

3.2 Effect of line length

For verification on its original test system, the 400 kV system of [33] was modelled, and its test cases were simulated in the time domain for line lengths of 50, 100, 200, 300 and 400 km with max(25, $\ell/10$) π-sections on each side of the fault, 0° inception and the recorder of Table 3. The method of [33] used the actual fault type, whereas the proposed method identified the fault type among 31 fault types. Table 8 gives the mean FLE of the proposed method. For the same test cases, the mean FLE reported in [33] is 0.004–0.019 % at d = 0.1, 0.030–0.387 % at d = 0.5 and 0.050–0.844 % at d = 0.9, and the method of [33] gives 0.002–0.020 %, 0.015–0.810 % and 0.046–2.63 %, respectively, with the largest values on the 400 km line. The proposed method gives 0.00001–0.0004 %, 0.0001–0.0070 % and 0.0008–0.043 % at the same distances.

The method of [33] shows the trends reported in [33]: its FLE increases with the fault distance and the line length. At 300–400 km and d $\geq$ 0.5, the values are two to three times higher than the values reported in [33], which is attributed to the different simulation tool and phasor window and to the decaying dc component remaining in the window. Over the 120 cases, the mean FLE of the method of [33] was 0.44 % (reported: 0.18 %) and its maximum 3.8 % (reported: 1.07 %); the original update

Table 8 Mean FLE (%) of the proposed method on the 400 kV system of [33]

d (p.u.)	50 km	100 km	200 km	300 km	400 km
0.1	0.0004	0.00001	0.0001	0.0003	0.0004
0.5	0.0001	0.0007	0.0010	0.0030	0.0070
0.9	0.0028	0.0008	0.0016	0.0086	0.043

Test cases of Table 1 of [33]: AG, BC, BCG and ABCG faults with two fault resistances each (eight cases per cell).

did not converge in 26 cases, all BC faults. The proposed method gave a mean FLE of 0.0048 %, a median of 0.0004 % and a maximum of 0.108 %, and it was more accurate in 116 of the 117 cases that it located; one ABCG fault at d = 0.1 on the 50 km line was reported as UNOBSERVABLE and two BC faults as AMBIGUOUS. For ABCG faults, the ungrounded three-phase topology was selected, because a balanced three-phase fault has no zero-sequence component and its ground connection cannot be identified from terminal data; the location is not affected.

The same comparison was performed on the 500 kV system for line lengths of 150, 200, 300 and 400 km with AG faults (R_F = 0.001, 80 and 320 Ω), BC faults (R_F = 0.001 and 40 Ω) and A1A2G faults at all eleven distances and 0° inception (88 cases per length, 55 of them observable). The 250 km values refer to the same 55 cases of the main study (Fig. 10 and Table 9).

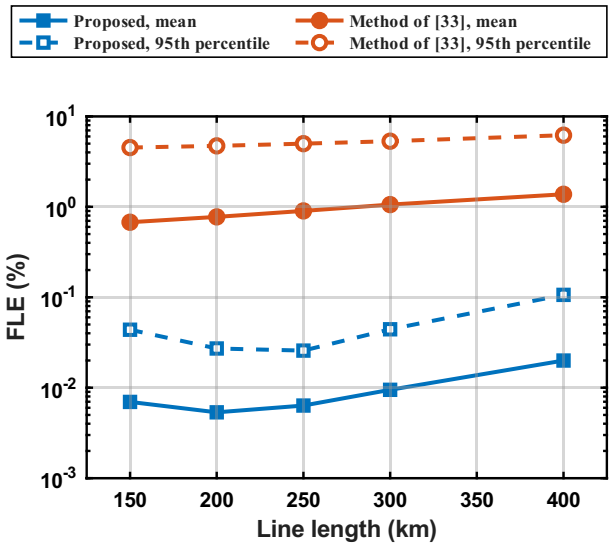


Fig. 10 Mean and 95th percentile FLE versus line length (55 observable faults per length)

As shown in Fig. 10, the median FLE of the method of [33] increases from 0.137 % at 150 km to 0.630 % at 400 km (mean 0.676 % to 1.38 %), and at 400 km only

Table 9 FLE (%) of the proposed method versus line length, 500 kV system

Length (km)	Cases	Type identified (%)	Distance valid (%)	Mean	Median	95th pct.	FLE < 1 % (%)
150	55	100.0	100.0	0.0070	0.0004	0.044	100.0
200	55	100.0	100.0	0.0053	0.0005	0.027	100.0
250	55	100.0	100.0	0.0063	0.0022	0.026	100.0
300	55	98.2	100.0	0.0093	0.0029	0.044	100.0
400	55	85.5	100.0	0.019	0.0038	0.078	100.0

FLE statistics over the distance-valid results.

58.2 % of its cases are located within 1 %, because the line charging and the remote infeed increase with the length. According to Table 9, the median FLE of the proposed method increases from 0.0004 % to 0.0038 % and is more than 150 times lower at every length, because the shunt capacitance is represented exactly in (3). At 400 km, eight of the 55 cases are type ambiguous, mostly between the same fault on circuit 1 and circuit 2 or with and without ground. Since both solutions give the same distance, all eight are reported as VALID-DISTANCE (median FLE 0.010 %, maximum 0.063 %), and all 55 cases are located within 1 %, against 85.5 % if they were reported as AMBIGUOUS. For the A1A2G faults, the method of [33] returned a distance in 52 of 132 cases, all with FLE > 1 % (median 13.0 %), whereas the proposed method reported them as UNOBSERVABLE. In the 211 cases in which both methods give a type-identified result, the proposed method is more accurate in 99.5 % (median ratio of the paired errors 0.0059, 95 % bootstrap interval 0.0050–0.0081).

3.3 Convergence and computation time

In [33], the convergence of the iterative distance update is examined for different initial values. The proposed method has no iterative update; its behaviour is described by the objective function $J_h(d)$ of (15) along the distance scan. Fig. 11 shows a) the objective function of the proposed method and b) the iterations of the method of [33] for initial values $\mathrm{d}^{(0)} = 0,\ 0.1,\ \ldots,\ 0.9$, for an AG fault with $R_F = 40\ \Omega$ at $\mathrm{d} = 0.2$, 0.5 and 0.8.

The objective function has a single sharp minimum at the actual fault location in all three cases, where $J(d)$ decreases by about eight orders of magnitude (7.7–8.5 decades), and no secondary minimum appears. The refined estimates are 0.20001, 0.49999 and 0.79999 p.u. (FLE 0.0006 %, 0.0009 % and 0.0011 %). Since the minimum is found by a global scan followed by a local refinement, the result does not depend on an initial value. The method of [33] converges in three, three and four iterations, independent of $d^{(0)}$, which confirms the behaviour reported in [33]; however, it converges to 0.1998, 0.4974 and 0.7903 p.u. (FLE 0.021 %, 0.262 % and 0.968 %). The converged point is biased because of the approximations in the update formula and the one-cycle phasors, and the bias increases with the fault distance.

The sensitivity of the estimate to the data window was examined for an AG fault at $\mathrm{d} = 0.5$ with $R_F = 20\ \Omega$ and 0° inception, in which the fault current increased from 610 A to 3237 A. When the residual (12) is evaluated with single one-cycle DFT

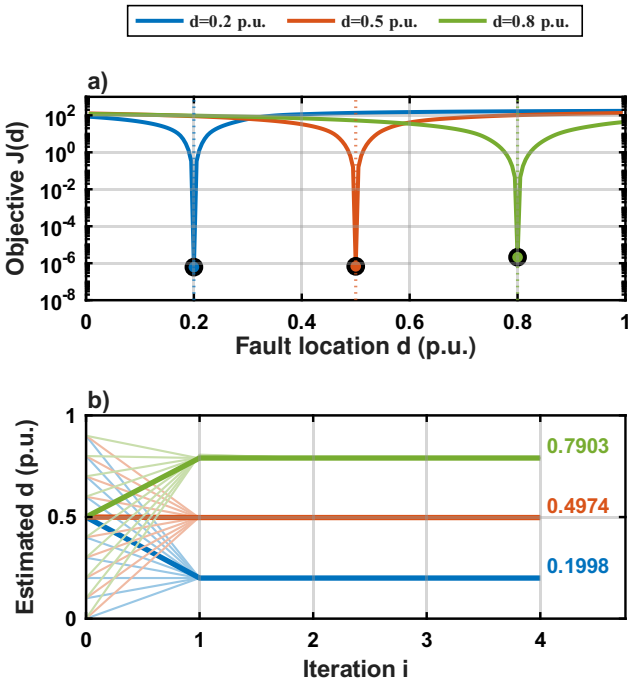


Fig. 11 a) Objective function of the proposed method; b) iterations of the method of [33] (AG fault, $R_F = 40\ \Omega$)

windows starting 27–39.5 ms after inception, the estimate varies between 0.49909 and 0.50035 p.u. (about 300 m), which shows that the one-cycle DFT phasor still contains part of the decaying dc component. The method of [33] gives 0.49651–0.49775 p.u. for the same windows, i.e. the same variation and an additional bias of about -2.5×10^{-3} p.u. (−630 m). With the phasor fit (5)–(7) and multiwindow fusion, the proposed method locates this fault with an error of 1.8×10^{-5} p.u. (4.5 m).

On a two-core laptop with MATLAB R2026a, the proposed method requires 6.7 s per case (median) including the 200-draw confidence interval, 1.5–4 s without it and 16 s with the joint skew estimation (25). The method of [33] requires 0.0025 s and is about three orders of magnitude faster; the computation time of the proposed method is mainly due to the scan over 31 topologies and the Monte Carlo interval. Since fault location is performed after fault clearing to dispatch the maintenance crew, a computation time of a few seconds is acceptable, and the 31 topology fits can be executed in parallel. For comparison, the state-space solver (21) required 6.0 s per case, and Simscape required 1254 s with 25 + 25 π-sections and 2432 s with 50 + 50 π-sections (medians).

3.4 Untransposed and nonidentical circuits

Since the proposed method uses the full 6×6 matrices in (1)–(3), no modification is required for untransposed or nonidentical circuits. To verify this, the untransposed,

nonidentical 200 km line of [33] was simulated with faults at d = 0.4 and fault resistances of 10, 30, 50, 70 and 100 Ω. The FLE of the proposed method is 0.0002–0.0034 % for AG, 0.0002–0.0008 % for BCG, 0.0001–0.0010 % for BC and 0.00001–0.00015 % for ABCG faults. For the same faults, the FLE reported in [33] is 0.635–0.757 % for AG, 0.363–0.504 % for BCG and 0.012–0.142 % for BC faults, and the method of [33] gives 0.022–0.199 % (mean 0.062 % against the reported 0.50 %); the original update failed for all five BC faults. The proposed method located all 20 faults (mean FLE 0.0004 %) and identified all fault types correctly, including the ground connection of the ABCG faults.

3.5 Effect of measurement noise

White Gaussian noise was added to all recorded voltages and currents before the antialiasing filter at signal-to-noise ratios (SNR) of 60, 40, 30 and 20 dB, defined for each channel relative to the rms value of its record. Fig. 12 shows a) the currents of circuit 1 with 30 dB noise for an AG fault with R_F = 100 Ω at d = 0.88 and b) the magnitude of the phase-A current phasor versus the window position obtained by the one-cycle DFT and by (5)–(7).

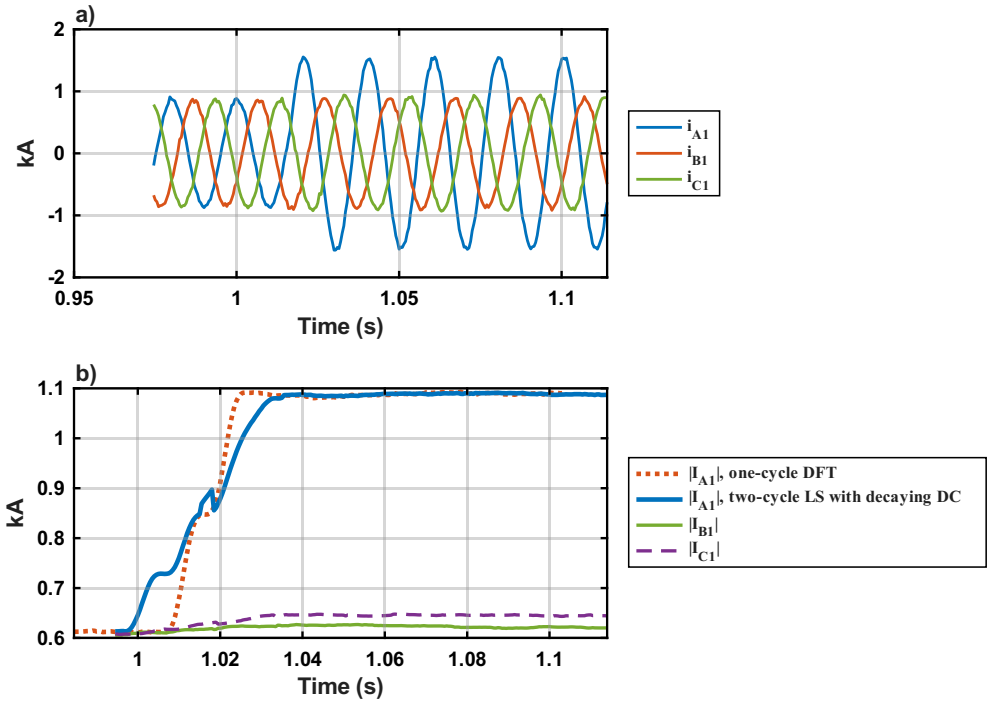


Fig. 12 a) Currents of circuit 1 with 30 dB noise; b) phase-A current phasor magnitude (AG fault, R_F = 100 Ω, d = 0.88 p.u.)

Because of the high fault resistance and the large distance, the current of the faulted phase increases only moderately, from 0.61 kA to 1.089 kA, while the healthy phases remain at about 0.62 kA and 0.65 kA. The estimate of (5)–(7) settles at the postfault value when the window centre is about 30 ms after inception, i.e. when the two-cycle window lies entirely after the inception and the filter has settled. After this time, the standard deviation of the magnitude is 1.2 A for the proposed estimator and 1.7 A for the one-cycle DFT, since the longer window and the decaying dc term reduce both the noise and the dc offset bias.

The noise study used 90 cases (all five fault types; d = 0.1, 0.5 and 0.9 p.u.; six fault resistances; 0° inception) with five noise realisations per SNR. The results below refer to the 72 observable cases (360 runs per SNR); the 18 A1A2G cases were reported as UNOBSERVABLE at every noise level. Fig. 13 shows the median FLE versus the fault location for each SNR.

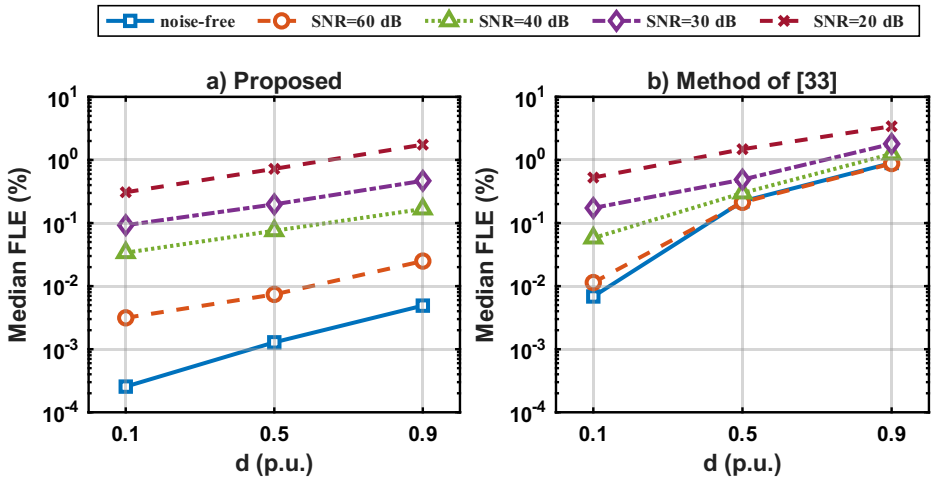


Fig. 13 Median FLE versus fault location for different SNR: a) proposed method; b) method of [33]

At d = 0.1, 0.5 and 0.9, the median FLE of the proposed method is 0.0031 %, 0.0074 % and 0.025 % at 60 dB, 0.093 %, 0.198 % and 0.467 % at 30 dB, and 0.308 %, 0.724 % and 1.75 % at 20 dB; the corresponding values of the method of [33] are 0.011 %, 0.213 % and 0.878 % at 60 dB, 0.173 %, 0.489 % and 1.80 % at 30 dB, and 0.526 %, 1.48 % and 3.42 % at 20 dB. Over all cases, the median FLE of the proposed method is 0.0090 %, 0.076 %, 0.199 % and 0.731 % at 60, 40, 30 and 20 dB, against 0.226 %, 0.352 %, 0.571 % and 1.26 % for the method of [33], i.e. lower by a factor of about 25, 4.6, 2.9 and 1.7. Up to 30 dB, the proposed method also locates more runs within 1 % (94.7 %, 79.4 % and 75.6 % at 60, 40 and 30 dB, against 82.5 %, 75.0 % and 64.4 %). With increasing noise, its share of valid results decreases to 85.0 % at 40 dB and 88.1 % at 30 dB, because some bolted faults are reported as AMBIGUOUS when the cross-circuit solution discussed in Section 2.4 can no longer be excluded. At 20 dB, 38 % of the runs are reported as AMBIGUOUS and 3 % as UNOBSERVABLE, and 36.1 % are located within 1 %, compared with 42.2 % for the method of [33],

which almost always returns a distance (94.4 % valid) but with a 95th percentile of 9.9 %. Under heavy noise, the proposed method therefore withholds uncertain results instead of returning large errors.

3.6 Effect of inception angle and sampling frequency

Every case of the main study was simulated with inception angles of 0°, 45° and 90°. For the observable fault types, the 95th percentile FLE of the proposed method is 0.017 %, 0.023 % and 0.021 % at the three angles, against 2.34 %, 2.51 % and 3.56 % for the method of [33], and its mean FLE is 0.0040 %, 0.0055 % and 0.0052 %. The inception angle has no systematic effect, which confirms that the dc model (5) removes the offset.

To examine the effect of the sampling frequency, AG faults with $R_F = 20\ \Omega$ at d = 0.1–0.9 p.u. were simulated with a time step corresponding to 51.2 kHz and recorded at 0.8, 1.6, 3.2, 6.4, 12.8 and 25.6 kHz with the same antialiasing filter, for inception angles of 0°, 45° and 90° (162 combinations). The results are shown in Fig. 14.

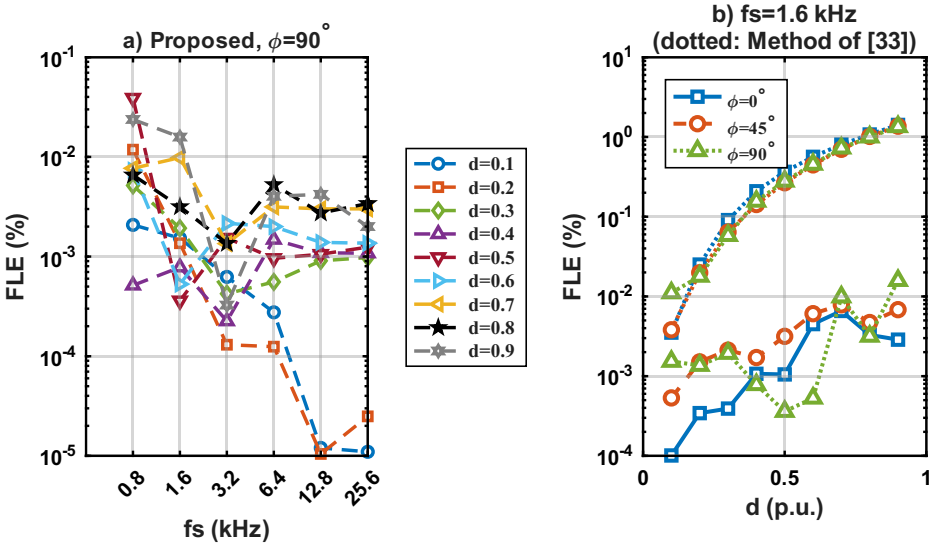


Fig. 14 a) FLE versus sampling frequency (90° inception); b) FLE versus fault location for different inception angles (f_s = 1.6 kHz)

The proposed method is practically insensitive to the sampling frequency and the inception angle: over all 162 combinations, its median FLE is 0.0014 % and its maximum 0.039 % (0.8 kHz, d = 0.5, 90°). For $f_s \geq 3.2$ kHz, all FLE values are at most 0.0063 %. The FLE decreases slightly from 0.8 to 3.2 kHz, because the two-cycle window contains more samples, and remains constant at higher frequencies. The FLE of the method of [33] is also practically independent of f_s and the inception angle, but it increases with the fault distance from about 0.005 % at d = 0.1 to 1.27–1.42 % at d = 0.9, with a median of 0.276 %.

3.7 Effect of line parameter errors

As in [33], the effect of uncertainty in the line capacitances was studied by a Monte Carlo analysis for an AG fault at d = 0.5 with R_F = 100 Ω, in which the self capacitances of each phase were varied randomly by ±2 % and the coupling capacitances by ±5 % in the estimator (200 draws). Both methods returned a location in all draws. The estimates of the proposed method lie between 0.49609 and 0.50319 p.u. (mean FLE 0.113 %, maximum 0.391 %), and those of the method of [33] between 0.49367 and 0.50035 p.u. (mean 0.264 %, maximum 0.633 %). Without a capacitance error, the FLE of the proposed method is 0.0013 % in this case, so random capacitance errors become its dominant error source, because the shunt currents are represented exactly in (3) and any error in them enters the residual (12). A common scaling of all capacitances by ±10 % has a much smaller effect (Table 10), because (10) depends mainly on the difference between the two circuits; random errors that differ between the circuits, as caused by different sag, conductor temperature or phase arrangement, are therefore more critical.

The sensitivity to the other line parameters was examined by changing the resistance, Z_0, Z_{0m} and the capacitance by ±10 % in the estimator only, for the cases at d = 0.5 p.u. with six fault resistances and 0° inception. The results for the 24 observable cases are given in Table 10; the six A1A2G cases were reported as UNOBSERVABLE in all tests.

Table 10 FLE (%) of the proposed method with line parameter errors

Parameter error	Cases	Valid (%)	Mean	Median	95th pct.	FLE < 1 % (%)
None	24	100.0	0.0026	0.0013	0.010	100.0
R −10 %	24	100.0	0.038	0.037	0.044	100.0
R +10 %	24	87.5	0.923	0.043	8.35	83.3
Z_0 −10 %	24	100.0	1.05	0.170	3.24	54.2
Z_0 +10 %	24	100.0	1.17	0.498	2.87	54.2
Z_{0m} −10 %	24	100.0	0.017	0.0085	0.055	100.0
Z_{0m} +10 %	24	100.0	0.017	0.0080	0.051	100.0
C −10 %	24	100.0	0.023	0.021	0.031	100.0
C +10 %	24	100.0	0.026	0.028	0.040	100.0
Z_0 −10 %, k_0 estimated	24	100.0	0.872	0.011	3.98	75.0
Z_0 +10 %, k_0 estimated	24	100.0	0.768	0.0043	3.49	75.0
Z_0 −3 % (after calibration)	24	100.0	0.445	0.194	1.80	91.7
Z_0 +3 % (after calibration)	24	100.0	0.411	0.202	1.24	95.8
Z_{0m} −3 %	24	100.0	0.0094	0.0047	0.034	100.0
Z_{0m} +3 %	24	100.0	0.016	0.0082	0.073	100.0

AG, BCG, BC and ABC faults, d = 0.5 p.u., six fault resistances, 0° inception.

The proposed method is insensitive to errors in the capacitance and the mutual impedance: a 10 % error changes its median FLE to 0.008–0.028 %, still 8 to 28 times lower than the error-free median of the method of [33] (0.221 %), and all cases remain within 1 %. The zero-sequence self-impedance has the largest effect, as for all single-ended methods on double-circuit lines [32]: a 10 % error in Z_0 increases the median

FLE of the proposed method to 0.170–0.498 % and that of the method of [33] to 0.287–0.987 %, and both methods locate only 50–54 % of the cases within 1 %, since grounded faults are affected and ungrounded faults are not. Two mitigations were evaluated (lower part of Table 10). First, Z_0 can be calibrated from earlier ground faults on the same line [32]; with a remaining error of ±3 % (±2 %), 92–96 % (88–92 %) of the cases are located within 1 %, the others being BCG faults with R_F = 80–320 Ω. Second, a common scale factor k_0 of the zero-sequence impedance (limited to ±25 %) can be estimated together with the distance; with a 10 % error in Z_0, this reduces the median FLE to 0.004–0.011 % and increases the share within 1 % from 54 % to 75 %, but not the 95th percentile, because k_0 cannot be identified for faults without zero-sequence current. A +10 % error in R makes three cases invalid and increases the mean FLE to 0.923 %, above that of the method of [33] (0.541 %), while the median remains 0.043 %; since this corresponds to a conductor temperature change of about 25 °C, a temperature-compensated resistance is advisable.

3.8 Effect of fault inductance

As in [33], the fault impedance was also modelled as a series resistance and inductance. The solver (21) was extended by a series R–L fault branch, and AG faults at d = 0.2 p.u. were simulated with R_F = 0.001, 10, 20, …, 100 Ω and L_F = 0.1, 0.5, 1, 2, 3 and 5 mH (66 cases, 0° inception). With a negligible inductance, the extended solver reproduced the phasors of the resistive solver within 7.8×10^{-6} (relative). Fig. 15 shows the FLE histograms of both methods.

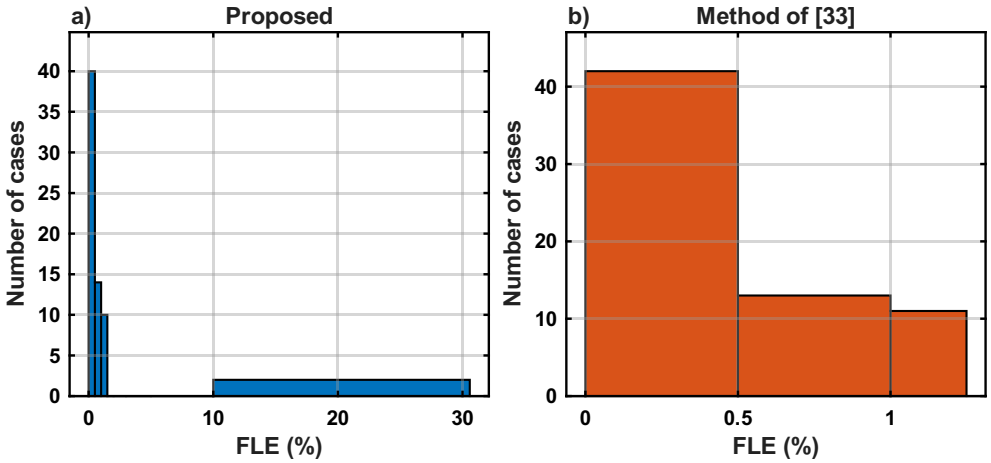


Fig. 15 FLE histogram for AG faults with R–L fault impedance: a) proposed method; b) method of [33]

Both methods model the fault path as purely resistive, so the fault reactance is interpreted as additional line reactance, and the FLE of both methods increases by about 0.25 % per millihenry. The median FLE of the proposed method is 0.025 %,

0.124 %, 0.246 %, 0.492 %, 0.738 % and 1.23 % for L_F = 0.1, 0.5, 1, 2, 3 and 5 mH, against 0.002 %, 0.099 %, 0.220 %, 0.462 %, 0.694 % and 1.17 % for the method of [33]; 82 % and 83 % of the 66 cases, respectively, are located within 1 %. In two cases with $R_F \approx 0$ and $L_F = 3$ and 5 mH, the fault is better matched by the bolted cross-circuit topology (Section 2.4), and the proposed method gives FLE values of 29.3 % and 30.6 %, whereas the method of [33], which uses the actual fault type, gives 0.38 % and 0.10 %. Two extensions of the fault model were tested on the tuning cases and rejected: an R–L variant of the phase-to-ground topologies reduced the residual by a factor of only 1.0–2.3, because a fault reactance changes the fault loop angle in the same way as the distance (Section 2.5), and a purely inductive bolted variant located two 5 Ω resistive faults on the other circuit at a wrong distance. An inductive fault impedance therefore remains a limitation, as for single-ended impedance-based methods in general.

3.9 Effect of prefault loading and unseen cases

The remote infeed depends on the prefault loading, which is the main error source of single-ended methods [6, 7]. Therefore, the load angle was changed from 15° to 5° and 30° (110 observable cases per load angle; Table 4). All cases are valid at all three load angles, and the median FLE of the proposed method is 0.0018 %, 0.0018 % and 0.0015 % at δ = 5°, 15° and 30°, with 95th percentiles of 0.025 %, 0.026 % and 0.023 %. The accuracy is thus independent of the loading, because the remote network enters the formulation only through (10). The median FLE of the method of [33] is 0.341–0.374 %, and 73.6–76.4 % of its cases are located within 1 %, whereas the proposed method locates all cases within 1 % (maximum 0.067 %). For the A1A2G faults, the method of [33] returned a distance in 27 of 66 cases with a median FLE of 21.2 %.

To exclude an adaptation to the grid of the main study, 30 unseen cases were simulated with distances (0.37, 0.63 and 0.88), resistances (55 and 230 Ω) and an inception angle (30°) that occur in no other case set. The proposed method located all 24 observable cases with a mean FLE of 0.0030 %, a median of 0.0022 % and a maximum of 0.0100 % (25 m), and it was more accurate than the method of [33] (mean 0.42 %, median 0.32 %) in all 24 cases. For the six A1A2G cases, the proposed method returned UNOBSERVABLE, whereas the method of [33] gave errors of 18.6 % and 42.4 % in two cases and a distance outside the line in the other four. Finally, 13 cases were simulated in Simscape with a finer model (50 + 50 π-sections, 5 μs step). For the nine observable faults, the FLE was 0.0004–0.12 % for the proposed method and 0.14–1.6 % for the method of [33], and the proposed method was more accurate in every case; the four A1A2G faults were reported as UNOBSERVABLE and were located by the source-assisted mode with FLE values of 0.0005–0.012 %.

3.10 Comparison

3.10.1 Qualitative comparison

Table 11 compares the features of the proposed method with those of the method of [33] and the reactance method [6]. In addition to the features of [33], the proposed method identifies the faulted circuit with a goodness-of-fit measure, uses dc-robust

phasors, detects unobservable faults and provides a confidence interval, at the cost of a computation time of a few seconds.

Table 11 Comparison of features

Feature	Takagi [6]	Method of [33]	Proposed
Measurements of one line end only	yes	yes	yes
Shunt capacitance and mutual coupling	no	yes	yes (exact)
Untransposed and nonidentical circuits	no	yes	yes
Fault type required as input	yes	no[a]	no
Faulted circuit identified with a goodness-of-fit measure	no	no	yes (BIC)
Distance obtained from	loop equation	fixed-point update	direct fit, all channels
Phasors robust to decaying dc	no	no	yes
Unobservable faults detected	no	no	yes
Confidence interval	no	no	yes
Instrument transformer correction, skew estimation	no	no	yes
Computation time per case	< 1 ms	a few ms	a few s

[a] In all comparisons of this paper, the actual fault type was supplied to the method of [33].

3.10.2 Quantitative comparison

For each combination of observable fault type and fault resistance in the main study, the mean FLE of the proposed method is 33–540 times lower than that of the method of [33]. The largest errors of the method of [33] occur for bolted faults (1.42–3.00 %) and decrease to 0.246–0.363 % at 320 Ω, whereas the proposed method gives 0.0007–0.014 % for all combinations. Fig. 16 shows the cumulative distribution of the FLE in the main study. The proposed method locates 69.8 % of all 990 cases within 0.01 % and 79.6 % within 0.1 %, compared with 9.6 % and 27.7 % for the method of [33]; within 1 %, the shares are 79.6 % and 67.8 %. The curve of the proposed method saturates at about 80 % because no distance is returned for the 198 A1A2G cases.

For the loading, line length and unseen sets, the median FLE of the method of [33] is 0.373 %, 0.285 % and 0.320 %, and 75.0 %, 73.2 % and 91.7 % of its cases are located within 1 %. In the cases in which both methods give a type-identified result, the proposed method is more accurate in 99.1 %, 99.5 %, 99.5 % and 100 % of the pairs in the main, loading, line length and unseen sets, with median ratios of the paired errors of 0.0075, 0.0071, 0.0059 and 0.0071 (95 % bootstrap intervals 0.0067–0.0089, 0.0056–0.0095, 0.0050–0.0081 and 0.0052–0.0093). Since the cases come from a structured grid, these effect sizes are more informative than significance tests; the Wilcoxon signed-rank test gives $p < 10^{-5}$ in every set. In the main study, the median error ratio of 0.0075 corresponds to an error about 130 times lower. Compared with the original update (median FLE 0.289 %), the proposed method is more accurate in 98.8 % of the 603 paired cases. The results of the proposed method for all case sets are summarised in Table 12.

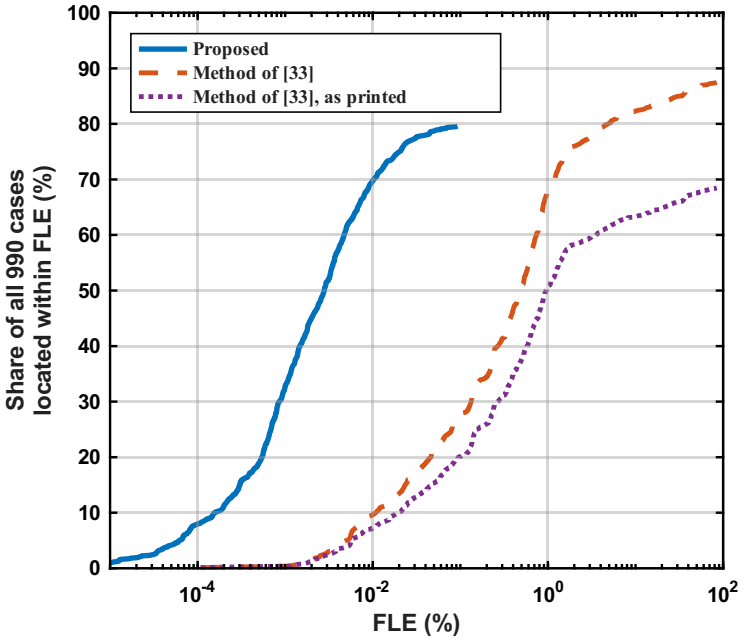


Fig. 16 Cumulative distribution of the FLE, main study (990 cases)

Table 12 Results of the proposed method for all case sets

Case set	Cases	Type identified	Distance valid	Mean FLE (%)	Median FLE (%)	95th pct. (%)	FLE $<$ 1 % (%)
Main	990	788	789	0.0049	0.0014	0.022	79.6
Loading	286	220	220	0.0056	0.0016	0.024	76.9
Line length	352	211	220	0.010	0.0012	0.049	59.9
Unseen	30	24	24	0.0030	0.0022	0.0097	80.0

All fault types; A1A2G faults are counted as not located. FLE $<$ 1 %: share of all cases with a type-identified result and FLE $<$ 1 %.

The proposed method also identifies the fault type and the faulted circuit, which were supplied to the method of [33]. Of the 792 observable faults of the main study, 788 (99.5 %) were located with the correct topology; no fault was located with a wrong topology, one ABC fault was ambiguous between the grounded and ungrounded three-phase topologies (with agreeing distances), and three BC faults with $R_F = 320$ Ω were reported as UNOBSERVABLE.

The coverage of the 95 % confidence interval is given in Table 13, and Fig. 17 shows the interval width versus the location error. Without the model bias term, the coverage was 94.3 % in the main study but only 89.5 % and 91.0 % in the loading and line length sets. In the main study, 38 of the 45 misses were bolted faults located by the model (16), whose Monte Carlo intervals are only a few metres wide because the noise

draws do not contain the deterministic difference between plant and model (about 1–120 m); most other misses were ungrounded faults with $R_F = 320\ \Omega$, whose intervals are not widened by the Z_0 uncertainty. With the model bias term, the coverage is 98.1–100 % in every set, while the median width changes by less than 1 %. The interval is therefore conservative. The intervals of resistive faults are a few kilometres wide because they include the assumed 5 % uncertainty of Z_0 and Z_{0m}; they indicate the line section to be inspected. Fig. 17a was obtained with $\epsilon_b = 10^{-3}$ (787 valid results).

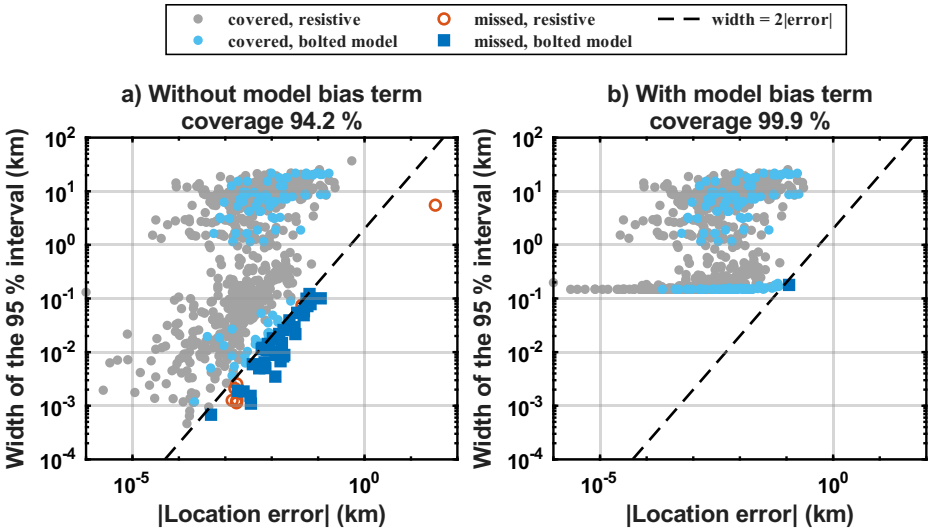


Fig. 17 Width of the 95 % confidence interval versus FLE: a) without and b) with the model bias term

Table 13 Coverage of the 95 % confidence interval

Case set	Valid cases	Coverage without bias term (%)	Coverage (%)	Median width (km)	Mean width (km)
Main, all	788	94.3	99.9	1.43	4.89
Main, grounded and ungrounded	593	93.4	99.8	5.45	6.38
Main, high resistance	195	96.9	100.0	0.15	0.36
Main, bolted-fault model	132	71.2	99.2	0.67	4.94
Loading	220	89.5	99.5	3.04	5.53
Line length	211	91.0	98.1	4.14	7.46
Unseen	24	100.0	100.0	3.91	5.69

3.10.3 Sources of the improvement

The improvement has three sources. First, the method of [33] updates the distance from the fault loop equation of one faulted phase, so the error of every approximation in this equation, such as the treatment of the remote infeed and the line charging, appears directly in the distance. The proposed method instead fits all channels of both circuits to the exact distributed-parameter model. With the same one-cycle DFT phasors, this alone reduces the median FLE from 0.221 % to 0.0030 % (Section 4.2), and it explains why the improvement is largest for remote faults, long lines and heavy loading. Second, the two-cycle least-squares fit with an exponential term removes the dc bias of the one-cycle DFT and, together with multiwindow fusion and the bolted-fault model, reduces the mean FLE by a further factor of about 40 and makes all bolted faults locatable. Third, the topology selection, the observability test and the confidence interval do not improve a correct estimate but make the result reliable: the faulted circuit is identified, a fault that cannot be located from one end is reported instead of being located with an error of 20 % or more, and the interval shows the section to be inspected. With several uncorrected measurement errors acting together, the advantage decreases to a factor of about 1.5, and with instrument transformer correction it is about 3.3 (Section 4.1). The noise-free factor of about 130 is therefore an upper bound for an exactly known line, and the improvement expected in practice is of the order of 1.5–4.

4 Robustness and discussion

4.1 Measurement errors

The tests in this section use the cases of Section 3.7 (d = 0.5 p.u., six fault resistances, 0° inception). The six A1A2G cases were reported as UNOBSERVABLE in all tests, and the results refer to the 24 observable cases, for which the proposed method gives a mean FLE of 0.0026 % and a median of 0.0013 % without disturbances, against 0.444 % and 0.221 % for the method of [33]. The results for instrument transformer errors and time skew are given in Table 14.

With moderate and severe current transformer (CT) saturation, the mean FLE of the proposed method increases from 0.0026 % to 0.014 % and 0.338 %, respectively, compared with 0.554 % and 1.37 % for the method of [33]; with severe saturation, 83.3 % and 75.0 % of the cases, respectively, are located within 1 %. A common gain error of 1 % on all voltages or all currents scales the apparent impedance and causes an almost constant error of 0.5 % at d = 0.5, which is of the same order as the error of the method of [33] under the same conditions (median 0.28–0.71 %) and is removed by routine calibration. A gain error on the circuit-2 currents only disturbs the balance between the circuits on which (10) is based, but its effect is moderate (median 0.069–0.089 %).

Since the residual (12) relates phasors of different channels, the uncorrected method is sensitive to time skew between them. A skew of 50 μs (0.9° at 50 Hz) between the currents and the voltages increases the median FLE to 1.37 %, and a skew of 200 μs to 5.40 %, slightly more than for the method of [33] (1.13 % and 4.06

Table 14 FLE (%) with instrument transformer errors and time skew

Disturbance	Cases	Valid (%)	Mean	Median	95th pct.	FLE < 1 % (%)
Instrument transformer errors within class limits (VT class 0.5, CT class 5P), five draws per case						
With certificate correction (23)	120	98.3	0.177	0.071	0.630	95.8
Uncorrected	120	97.5	1.50	0.522	4.92	62.5
Method of [33], corrected / uncorrected	120	100 / 100	0.506 / 2.04	0.237 / 1.09	2.99 / 7.44	90.0 / 48.3
Single error sources, uncorrected						
None	24	100.0	0.0026	0.0013	0.010	100.0
All voltages -1 %	24	100.0	0.498	0.497	0.504	100.0
All voltages $+1$ %	24	100.0	0.494	0.496	0.499	100.0
All currents -1 %	24	100.0	0.499	0.501	0.504	100.0
All currents $+1$ %	24	100.0	0.493	0.492	0.499	100.0
Circuit-2 currents -1 %	24	100.0	0.167	0.089	0.626	100.0
Circuit-2 currents $+1$ %	24	95.8	0.145	0.069	0.631	95.8
Currents vs voltages, 50 μs, without / with skew estimation	24	87.5 / 87.5	2.53 / 2.10	1.37 / 0.757	10.7 / 10.6	33.3 / 45.8
Currents vs voltages, 200 μs, without / with skew estimation	24	87.5 / 87.5	7.38 / 5.68	5.40 / 2.95	17.7 / 17.5	0.0 / 20.8
Circuit 2 vs circuit 1, 50 μs, without / with skew estimation	24	87.5 / 100	1.47 / 0.0026	0.435 / 0.0013	7.07 / 0.011	58.3 / 100
Circuit 2 vs circuit 1, 200 μs, without / with skew estimation	24	91.7 / 100	4.58 / 0.023	1.44 / 0.0015	18.7 / 0.155	37.5 / 100

Proposed method unless stated; observable fault types, d = 0.5 p.u.

%). A phase displacement between the voltage and current transformers has the same effect and is of this order for protection-class transformers; its correction is described in Section 4.1.1. A skew between the two circuits affects both methods to a similar degree without correction (median 0.435 % and 1.44 % for the proposed method, against 0.623 % and 1.96 % for the method of [33] at 50 μs and 200 μs). When 30 dB noise, a $+10$ % error in Z_{0m}, a $+1$ % current gain error and moderate CT saturation were applied together (24 cases, five noise realisations), the proposed method gave a median FLE of 0.584 % (mean 0.802 %, 95.0 % valid) and located 74.2 % of the runs within 1 %, against 0.903 % (mean 1.41 %) and 57.5 % for the method of [33]. Without correction, the advantage therefore decreases to a factor of about 1.5.

4.1.1 Instrument transformer correction and time skew estimation

The ratio and phase errors of each voltage and current transformer are known from its test certificate or from commissioning tests. Before Stage 1, each channel phasor is therefore divided by its complex correction factor:

$$X_{ch} \leftarrow X_{ch}/k_{ch}, \qquad k_{ch} = (1 + \varepsilon_{ch})\, e^{j\varphi_{ch}} \tag{23}$$

where ε_{ch} and φ_{ch} are the certified ratio and phase errors. A remaining time skew Δ_{21} between the currents of circuit 2 and circuit 1 is estimated from the prefault state. Since both healthy circuits terminate at bus R, the receiving-end voltages calculated through the two circuits from the prefault phasors (least-squares sine fit over five cycles ending 2 ms before inception) must be equal:

$$\hat{\Delta}_{21} = \arg \min_{|\Delta| \le 300\,\mu\mathrm{s}} \left\| \mathbf{E}\,\mathbf{T}(\ell)\,[\mathbf{v}_S;\ \mathbf{v}_S;\ \mathbf{i}_1;\ \mathbf{i}_2 e^{j\omega\Delta}]_{\mathrm{pre}} \right\|^2 \tag{24}$$

and the circuit-2 currents are rotated by $e^{j\omega\hat{\Delta}_{21}}$. A skew Δ_{IV} between all currents and the voltages does not change the prefault mismatch and must be estimated with the fault. It enters (12) as one additional real unknown:

$$\mathbf{I}_S \leftarrow \mathbf{I}_S\, e^{j\omega\Delta_{IV}}, \qquad (\hat{d}, \hat{\boldsymbol{\theta}}, \hat{\Delta}_{IV}) = \arg\min J_h(d, \boldsymbol{\theta}, \Delta_{IV}) \tag{25}$$

which is solved by evaluating the unweighted mismatch over Δ_{IV} on a 50 μs grid followed by refinement. The estimate is used only if it is identifiable, i.e. if a shift of ± 50 μs from the optimum at least doubles the mismatch; otherwise, the calibrated value is kept. In the tests, Δ_{IV} was identifiable only for phase-to-phase-to-ground faults, for which a ± 50 μs shift increased the mismatch by a factor of 20–850, whereas for phase-to-ground, phase-to-phase and three-phase faults the factor was 0.6–1.4, i.e. skew and distance compensate each other almost exactly (Section 2.5). After correction by (23), the remaining skew is small and the search in (25) is limited to ± 25 μs; without this limit, a zero-sequence impedance error was partly interpreted as a skew of 18–243 μs for phase-to-phase-to-ground faults.

To evaluate the correction, ratio and phase errors were drawn uniformly within the limits of protection-class transformers (VT class 0.5: ± 0.5 %, ± 20'; CT class 5P: ± 1 %, $\pm 60' \approx 56$ μs) for every channel, with five draws per case, and applied to the recorded waveforms; the estimator used certificate values with a remaining uncertainty of ± 0.1 % in ratio and ± 5 μs in phase. The results are given in Table 14. Without correction, the median FLE of the proposed method is 0.522 % and 62.5 % of the runs are located within 1 % (method of [33]: 1.09 % and 48.3 %). With certificate correction, the median FLE decreases to 0.071 %, 95.8 % of the runs are located within 1 %, and the proposed method is about 3.3 times more accurate than the method of [33] with the same corrected phasors (0.237 %). The circuit-to-circuit skew is removed completely by (24): for 50 μs and 200 μs, the median FLE is 0.0013 % and 0.0015 %, as without skew, and all cases are valid. Without correction, the joint estimation (25) recovers a current-to-voltage skew within 1 μs for phase-to-phase-to-ground faults (FLE ≤ 0.003 %) and approximately halves the median FLE over all fault types (0.757 % and 2.95 % at 50 μs and 200 μs), which is lower than for the method of [33]. The remaining error comes from the single-loop fault types, for which the correction (23) is required.

4.2 Contribution of the components

To separate the contributions of the location equations and of the phasor estimator, the proposed location equations were combined with different phasor estimators (Table 15).

Table 15 FLE (%) of the proposed location equations with different phasor estimators

Phasor estimator	Valid (%)	Mean	Median	95th pct.	FLE < 1 % (%)
One-cycle DFT [38] (as in [33])	45.8	0.113	0.0030	0.987	41.7
Two-cycle DFT	54.2	0.292	0.0025	2.19	50.0
Mimic filter + DFT [39]	54.2	0.105	0.055	0.411	54.2
One-cycle DFT with dc removal, τ on a grid [42]	66.7	0.034	0.0065	0.234	66.7
Multiwindow one-cycle DFT	91.7	0.160	0.0029	1.58	83.3
Proposed (5)–(7), multiwindow, with bolted-fault model	100.0	0.0026	0.0013	0.010	100.0

24 observable cases, d = 0.5 p.u.; without the bolted-fault model unless stated.

With the same one-cycle DFT phasors as the method of [33], the proposed location equations reduce the median FLE from 0.221 % to 0.0030 %, i.e. by a factor of about 70, and the mean from 0.444 % to 0.113 %. This results from solving the full six-conductor distributed-parameter model directly instead of iterating the fault loop equation of one phase. The factor of 70 is an upper estimate, because only 45.8 % of the cases are located with these phasors (41.7 % within 1 %, against 91.7 % for the method of [33]); many bolted faults cannot be located, and the mimic filter and the dc removal with a grid of time constants improve this only partly. The proposed least-squares fit with an optimised time constant, together with multiwindow fusion and the bolted-fault model, locates all 24 cases and reduces the mean FLE by a further factor of about 40, to 0.0026 %; with one-cycle DFT phasors, none of the four bolted faults is located within 1 %, whereas with the proposed estimator all four are. In an ablation study, in which the components were added one at a time to a baseline with single-window least-squares phasors, the actual fault type, a lumped π-section line model and a local search, the unknown fault type was the most demanding step, because for bolted faults a cross-circuit topology at a different distance fits almost equally well. The distance scan, the weights and the Huber function removed these wrong solutions at the cost of more ambiguous results, and multiwindow fusion and the bolted-fault model increased the share of valid results to 100 %. Estimating a zero-sequence compensation factor k_0 together with the distance degraded the results when the line parameters were correct and is therefore used only when Z_0 is uncertain (Table 10). With 30 dB noise and a 10 % error in Z_{0m}, the complete method gave a mean FLE of 0.555 %, about 1.4 times lower than the method of [33] (0.804 %).

4.3 Limitations

All results were obtained by simulation. The plant consisted of lumped π-sections, and an independent Simscape model with twice as many sections confirmed the results for 13 cases. Frequency-dependent line parameters and instrument transformer transients were not modelled, and the plant and the estimator use the same per-unit-length parameters; the noise-free accuracy is therefore an upper bound for an exactly known line. Validation with a frequency-dependent electromagnetic transient model and with recorded field data is the most important next step. Further limitations are: (a) a 10 % error in Z_0 leaves only 54 % of the cases within 1 %, which calibration to ±3 %

increases to 92–96 % (Table 10); (b) a current-to-voltage skew can be estimated only for phase-to-phase-to-ground faults, so for the other fault types the remaining skew after calibration determines the error (uncorrected 0.3–3.9 % at 50 μs for R_F = 20–320 Ω and d = 0.5); (c) an inductive fault impedance causes an error of about 0.25 % per millihenry, as for the method of [33] (Section 3.8); (d) the method requires both circuits in service between common buses and a record of 79.5 ms after inception without breaker operation; (e) the inception time was assumed to be known, and a fault detector was not evaluated; (f) the tests covered AG, BC, BCG, ABC and A1A2G faults on circuit 1 (and ABCG faults on the 400 kV system) with equal branch resistances, while the other cross-circuit faults, circuit-2 faults and faults outside the 31 fault types were not simulated; (g) the robustness, noise and high-fidelity studies used reduced case sets (13–90 cases, five noise realisations), and the noise study, the phasor estimator comparison (Table 15), the ablation, the ±10 % R, Z_{0m} and C cases of Table 10, the gain error cases of Table 14 and the CT saturation and combined error tests were performed with $\epsilon_b = 10^{-3}$, without the model bias term and without the distance agreement rule. Evolving and arcing faults, series-compensated lines and multiterminal lines were not considered, and the comparison is limited to one method.

5 Conclusion

A single-ended fault location method for double-circuit transmission lines without a fixed-point distance update has been presented. The fault distance and the fault path conductances are estimated jointly from the common-bus residual of the exact six-conductor distributed-parameter model; the fault type and the faulted circuit are identified among 31 fault types by the Bayesian information criterion; unobservable faults are detected; the phasors are obtained by a dc-robust two-cycle least-squares fit over several windows; instrument transformer errors and time skew are corrected; and a 95 % confidence interval is provided. The method was evaluated on 1658 fault cases of a 500 kV double-circuit line of 150–400 km and on the test cases of [33], with the method of [33] applied to the same waveforms. The main conclusions are:

- In the 990 noise-free cases of the main study, the median FLE was 0.0014 % (3.5 m) against 0.270 % for the method of [33]; the proposed method was more accurate in 99.1 % of the paired cases, and none of its 1243 type-identified locations in all case sets had an FLE above 0.3 %.
- On the test system of [33], the maximum FLE was 0.108 % against 3.8 %; untransposed and nonidentical circuits required no modification, and the accuracy depended little on the fault resistance, the inception angle, the line length (150–400 km) and the load angle (5–30°), which was confirmed on unseen cases.
- The fault type and the faulted circuit were identified correctly for 99.5 % of the tested observable faults, circuit-symmetric faults were reported as unobservable, and the coverage of the 95 % confidence interval was 98.1–100 % in all case sets.
- With the same one-cycle phasors as the method of [33], the proposed location equations alone reduced the median FLE by a factor of about 70; the dc-robust phasor estimator with multiwindow fusion and the bolted-fault model reduced the mean FLE by a further factor of about 40.

- With protection-class instrument transformer errors, the median FLE was 0.071 % with certificate correction (95.8 % of the runs within 1 %), against 0.237 % for the method of [33] with the same correction; without correction, it was 0.52 % against 1.09 %.

The main remaining error sources are errors in the zero-sequence impedance, for which calibration from recorded ground faults is recommended, an inductive fault impedance and an uncorrected current-to-voltage skew for single-loop faults. Future work will address validation with a frequency-dependent electromagnetic transient model and field records, operation with the parallel circuit out of service and with short records, and series-compensated and multiterminal lines.

Declarations

Funding. Not applicable.

Competing interests. The authors declare no competing interests.

Clinical trial registration. Not applicable. This study does not involve a clinical trial.

Ethics approval and consent to participate. Not applicable. This study did not involve human participants or animal experiments.

Consent for publication. Not applicable.

Data availability. All data generated or analysed during this study are included in this published article.

Author contributions. Abhay Yadav conceived the study, developed the methodology, wrote the software, performed the simulations, carried out the formal analysis and investigation, prepared the visualizations and wrote the original draft of the manuscript. Soma Deb and V. P. Singh supervised the work, checked and validated the methodology and the results, and reviewed and edited the manuscript. All authors read and approved the final manuscript

Appendix A Distance update of the method of Khodadadi Arpanahi et al.

The method of [33] updates the distance from the fault loop equation of one faulted phase p. With the sending-end phase voltages $\mathbf{V}_S$, the voltage drop per unit distance $\mathbf{V}_L$ of the faulted circuit obtained in its first subproblem and the estimated fault currents $\mathbf{I}_F$, the fault-point voltage is $\mathbf{V}_F = \mathbf{V}_S - d\,\mathbf{V}_L$. For a phase-to-ground fault, the update follows from the condition that the fault resistance is real, $\mathrm{Im}\{V_{F,p} I^{*}_{F,p}\} = 0$:

$$d^{(k+1)} = \frac{\mathrm{Im}\{V_{S,p}\, I^{*}_{F,p}\}}{\mathrm{Im}\{V_{L,p}\, I^{*}_{F,p}\}} \tag{A1}$$

For a phase-to-phase fault between phases p and q, $V_{F,p} - V_{F,q} = R_F I_{F,p}$ with a real R_F. The original update of [33] (Eq. (21) in [33]) uses the fault-point voltage of phase q from the previous iteration k:

$$d^{(k+1)} = \frac{\mathrm{Im}\{(V_{S,p} - V_{F,q}^{(k)})\, I_{F,p}^{*}\}}{\mathrm{Im}\{V_{L,p}\, I_{F,p}^{*}\}} \tag{A2}$$

Since $V_{F,q}^{(k)}$ depends on the distance of the previous iteration, the gain of this iteration is close to one, and in the present simulations it converged slowly or not at all (26 of the 120 cases of [33], all BC faults, and 94.9 % of the BC cases of the main study). Substituting $V_F = V_S - d\, V_L$ for both phases gives a rearranged form with the same fixed point:

$$d^{(k+1)} = \frac{\mathrm{Im}\{(V_{S,p} - V_{S,q})\, I_{F,p}^{*}\}}{\mathrm{Im}\{(V_{L,p} - V_{L,q})\, I_{F,p}^{*}\}} \tag{A3}$$

in which the previous distance enters only through $\mathbf{I}_F$ and $\mathbf{V}_L$. The rearranged form converged in 1–5 iterations in all cases, in agreement with the two to three iterations reported in [33], and where both forms converge they give the same distance. In this paper, the method of [33] uses (A3) unless stated otherwise; all other equations of [33] were implemented as published.

References

[1] Lopes FV. Settings-free traveling-wave-based earth fault location using unsynchronized two-terminal data. IEEE Trans Power Del. 2016;31(5):2296–2298. https://doi.org/10.1109/TPWRD.2016.2551367.

[2] Naidu OD, Pradhan AK. Precise traveling wave-based transmission line fault location method using single-ended data. IEEE Trans Ind Informat. 2021;17(8):5197–5207. https://doi.org/10.1109/TII.2020.3027584.

[3] Korkali M, Lev-Ari H, Abur A. Traveling-wave-based fault-location technique for transmission grids via wide-area synchronized voltage measurements. IEEE Trans Power Syst. 2012;27(2):1003–1011. https://doi.org/10.1109/TPWRS.2011.2176351.

[4] Chen K, Huang C, He J. Fault detection, classification and location for transmission lines and distribution systems: A review on the methods. High Voltage. 2016;1(1):25–33. https://doi.org/10.1049/hve.2016.0005.

[5] Mohammadi Shakiba F, Azizi SM, Zhou M, Abusorrah A. Application of machine learning methods in fault detection and classification of power transmission lines: A survey. Artif Intell Rev. 2023;56(7):5799–5836. https://doi.org/10.1007/s10462-022-10296-0.

[6] Takagi T, Yamakoshi Y, Yamaura M, Kondow R, Matsushima T. Development of a new type fault locator using the one-terminal voltage and current data.

IEEE Trans Power App Syst. 1982;PAS-101(8):2892–2898. https://doi.org/10.1109/TPAS.1982.317615.

[7] Eriksson L, Saha MM, Rockefeller GD. An accurate fault locator with compensation for apparent reactance in the fault resistance resulting from remote-end infeed. IEEE Trans Power App Syst. 1985;PAS-104(2):423–436. https://doi.org/10.1109/TPAS.1985.319058.

[8] Das S, Santoso S, Gaikwad A, Patel M. Impedance-based fault location in transmission networks: Theory and application. IEEE Access. 2014;2:537–557. https://doi.org/10.1109/ACCESS.2014.2323353.

[9] Didehvar S, Mohammadi Chabanloo R. Accurate estimating remote end equivalent impedance for adaptive one-ended fault location. Electr Power Syst Res. 2019;170:194–204. https://doi.org/10.1016/j.epsr.2019.01.011.

[10] Luo J, Liu YZ, Cui Q, Zhong J, Zhang L. Single-ended time domain fault location based on transient signal measurements of transmission lines. Protection and Control of Modern Power Systems. 2024;9(2):61–74. https://doi.org/10.23919/PCMP.2023.000503.

[11] Sachdev MS, Agarwal R. A technique for estimating transmission line fault locations from digital impedance relay measurements. IEEE Trans Power Del. 1988;3(1):121–129. https://doi.org/10.1109/61.4237.

[12] Girgis AA, Hart DG, Peterson WL. A new fault location technique for two- and three-terminal lines. IEEE Trans Power Del. 1992;7(1):98–107. https://doi.org/10.1109/61.108895.

[13] Novosel D, Hart DG, Udren E, Garitty J. Unsynchronized two-terminal fault location estimation. IEEE Trans Power Del. 1996;11(1):130–138. https://doi.org/10.1109/61.484009.

[14] Johns AT, Jamali S. Accurate fault location technique for power transmission lines. IEE Proc C–Gener Transm Distrib. 1990;137(6):395–402. https://doi.org/10.1049/ip-c.1990.0054.

[15] Gopalakrishnan A, Kezunovic M, McKenna SM, Hamai DM. Fault location using the distributed parameter transmission line model. IEEE Trans Power Del. 2000;15(4):1169–1174. https://doi.org/10.1109/61.891498.

[16] Jiang JA, Yang JZ, Lin YH, Liu CW, Ma JC. An adaptive PMU based fault detection/location technique for transmission lines. I. Theory and algorithms. IEEE Trans Power Del. 2000;15(2):486–493. https://doi.org/10.1109/61.852973.

[17] Izykowski J, Rosolowski E, Balcerek P, Fulczyk M, Saha MM. Accurate noniterative fault location algorithm utilizing two-end unsynchronized measurements.

IEEE Trans Power Del. 2010;25(1):72–80. https://doi.org/10.1109/TPWRD.2009.2035222.

[18] Salehi Dobakhshari A. Noniterative parameter-free fault location on untransposed single-circuit transmission lines. IEEE Trans Power Del. 2017;32(3):1636–1644. https://doi.org/10.1109/TPWRD.2017.2650780.

[19] Lu D, Liu Y, Liao Q, Wang B, Huang W, Xi X. Time-domain transmission line fault location method with full consideration of distributed parameters and line asymmetry. IEEE Trans Power Del. 2020;35(6):2651–2662. https://doi.org/10.1109/TPWRD.2020.2974294.

[20] Kawady T, Stenzel J. A practical fault location approach for double circuit transmission lines using single end data. IEEE Trans Power Del. 2003;18(4):1166–1173. https://doi.org/10.1109/TPWRD.2003.817503.

[21] Izykowski J, Rosolowski E, Saha MM. Locating faults in parallel transmission lines under availability of complete measurements at one end. IEE Proc–Gener Transm Distrib. 2004;151(2):268–273. https://doi.org/10.1049/ip-gtd:20040163.

[22] Chaiwan P, Kang N, Liao Y. New accurate fault location algorithm for parallel transmission lines using local measurements. Electr Power Syst Res. 2014;108:68–73. https://doi.org/10.1016/j.epsr.2013.11.001.

[23] Ramar K, Low HS, Ngu EE. One-end impedance based fault location in double-circuit transmission lines with different configurations. Int J Electr Power Energy Syst. 2015;64:1159–1165. https://doi.org/10.1016/j.ijepes.2014.09.006.

[24] Ghorbani A, Mehrjerdi H. Negative-sequence network based fault location scheme for double-circuit multi-terminal transmission lines. IEEE Trans Power Del. 2019;34(3):1109–1117. https://doi.org/10.1109/TPWRD.2019.2906056.

[25] Ghorbani A, Mehrjerdi H. Accurate fault location algorithm for shunt-compensated double circuit transmission lines using single end data. Int J Electr Power Energy Syst. 2020;116:105515. https://doi.org/10.1016/j.ijepes.2019.105515.

[26] Nemati M, Bigdeli M, Ghorbani A, Mehrjerdi H. Accurate fault location element for series compensated double-circuit transmission lines utilizing negative-sequence phasors. Electr Power Syst Res. 2021;194:107064. https://doi.org/10.1016/j.epsr.2021.107064.

[27] Duan M, Ye A, Liu Y. Partially coupled transmission line fault location using single-ended measurements. Electr Power Syst Res. 2024;233:110496. https://doi.org/10.1016/j.epsr.2024.110496.

[28] Korres GN, Apostolopoulos CA. Precise fault location algorithm for double-circuit transmission lines using unsynchronised measurements from two anti-parallel ends. IET Gener Transm Distrib. 2010;4(7):824–835. https://doi.org/10.1049/iet-gtd.2009.0533.

[29] Apostolopoulos CA, Korres GN. A novel fault-location algorithm for double-circuit transmission lines without utilizing line parameters. IEEE Trans Power Del. 2011;26(3):1467–1478. https://doi.org/10.1109/TPWRD.2010.2102777.

[30] Apostolopoulos CA, Korres GN. Accurate fault location algorithm for double-circuit series compensated lines using a limited number of two-end synchronized measurements. Int J Electr Power Energy Syst. 2012;42(1):495–507. https://doi.org/10.1016/j.ijepes.2012.03.042.

[31] Kang N, Liao Y. Double-circuit transmission-line fault location utilizing synchronized current phasors. IEEE Trans Power Del. 2013;28(2):1040–1047. https://doi.org/10.1109/TPWRD.2013.2246587.

[32] Salehi Dobakhshari A, Azizi S. On estimation of zero-sequence impedances of parallel transmission lines from fault data. IEEE Trans Power Del. 2025;40(2):831–842. https://doi.org/10.1109/TPWRD.2025.3527738.

[33] Khodadadi Arpanahi M, Hajiakbari Fini M, Nateghi A. A novel single-end fault location method for double-circuit transmission lines. Int J Electr Power Energy Syst. 2024;158:109984. https://doi.org/10.1016/j.ijepes.2024.109984.

[34] Gracia J, Mazón AJ, Zamora I. Best ANN structures for fault location in single- and double-circuit transmission lines. IEEE Trans Power Del. 2005;20(4):2389–2395. https://doi.org/10.1109/TPWRD.2005.855482.

[35] Jamehbozorg A, Shahrtash SM. A decision tree-based method for fault classification in double-circuit transmission lines. IEEE Trans Power Del. 2010;25(4):2184–2189. https://doi.org/10.1109/TPWRD.2010.2050911.

[36] Swetapadma A, Yadav A. All shunt fault location including cross-country and evolving faults in transmission lines without fault type classification. Electr Power Syst Res. 2015;123:1–12. https://doi.org/10.1016/j.epsr.2015.01.014.

[37] Swetapadma A, Yadav A. Directional relaying using support vector machine for double circuit transmission lines including cross-country and inter-circuit faults. Int J Electr Power Energy Syst. 2016;81:254–264. https://doi.org/10.1016/j.ijepes.2016.02.034.

[38] Phadke AG, Thorp JS. Synchronized Phasor Measurements and Their Applications. 2nd ed. Power Electronics and Power Systems. Cham, Switzerland: Springer; 2017. DOI: 10.1007/978-3-319-50584-8.

[39] Benmouyal G. Removal of DC-offset in current waveforms using digital mimic filtering. IEEE Trans Power Del. 1995;10(2):621–630. https://doi.org/10.1109/61.400869.

[40] Gu JC, Yu SL. Removal of DC offset in current and voltage signals using a novel Fourier filter algorithm. IEEE Trans Power Del. 2000;15(1):73–79. https://doi.org/10.1109/61.847231.

[41] Guo Y, Kezunovic M, Chen D. Simplified algorithms for removal of the effect of exponentially decaying DC-offset on the Fourier algorithm. IEEE Trans Power Del. 2003;18(3):711–717. https://doi.org/10.1109/TPWRD.2003.813894.

[42] Sidhu TS, Zhang X, Albasri F, Sachdev MS. Discrete-Fourier-transform-based technique for removal of decaying DC offset from phasor estimates. IEE Proc–Gener Transm Distrib. 2003;150(6):745–749. https://doi.org/10.1049/ip-gtd:20030943.

[43] de la O Serna JA. Dynamic phasor estimates for power system oscillations. IEEE Trans Instrum Meas. 2007;56(5):1648–1657. https://doi.org/10.1109/TIM.2007.904546.

[44] Nam SR, Park JY, Kang SH, Kezunovic M. Phasor estimation in the presence of DC offset and CT saturation. IEEE Trans Power Del. 2009;24(4):1842–1849. https://doi.org/10.1109/TPWRD.2008.2002972.

[45] Jiang Z, Miao S, Liu P. A modified empirical mode decomposition filtering-based adaptive phasor estimation algorithm for removal of exponentially decaying DC offset. IEEE Trans Power Del. 2014;29(3):1326–1334. https://doi.org/10.1109/TPWRD.2014.2299808.

[46] Afrandideh S, Haghjoo F. A DFT-based phasor estimation method robust to primary and secondary decaying DC components. Electr Power Syst Res. 2022;208:107907. https://doi.org/10.1016/j.epsr.2022.107907.

[47] Hajimahani MK, Zamani H, Jamali S. Data window selection for removal of decaying DC component in current phasor estimation for distance protection. Electr Power Syst Res. 2023;223:109546. https://doi.org/10.1016/j.epsr.2023.109546.

[48] Liao Y, Kezunovic M. Optimal estimate of transmission line fault location considering measurement errors. IEEE Trans Power Del. 2007;22(3):1335–1341. https://doi.org/10.1109/TPWRD.2007.899554.

[49] Korkali M, Abur A. Robust fault location using least-absolute-value estimator. IEEE Trans Power Syst. 2013;28(4):4384–4392. https://doi.org/10.1109/TPWRS.2013.2264535.

[50] Salehi Dobakhshari A, Ranjbar AM. A novel method for fault location of transmission lines by wide-area voltage measurements considering measurement errors. IEEE Trans Smart Grid. 2015;6(2):874–884. https://doi.org/10.1109/TSG.2014.2322977.

[51] Fu J, Song G, De Schutter B. Influence of measurement uncertainty on parameter estimation and fault location for transmission lines. IEEE Trans Autom Sci Eng. 2021;18(1):337–345. https://doi.org/10.1109/TASE.2020.2992236.

[52] Davoudi M, Sadeh J, Kamyab E. Parameter-free fault location for transmission lines based on optimisation. IET Gener Transm Distrib. 2015;9(11):1061–1068. https://doi.org/10.1049/iet-gtd.2014.0425.

[53] Kang YC, Lim UJ, Kang SH, Crossley PA. Compensation of the distortion in the secondary current caused by saturation and remanence in a CT. IEEE Trans Power Del. 2004;19(4):1642–1649. https://doi.org/10.1109/TPWRD.2004.835266.

[54] Mili L, Cheniae MG, Vichare NS, Rousseeuw PJ. Robust state estimation based on projection statistics. IEEE Trans Power Syst. 1996;11(2):1118–1127. https://doi.org/10.1109/59.496203.

[55] Zhao J, Wang S, Mili L, Amidan B, Huang R, Huang Z. A robust state estimation framework considering measurement correlations and imperfect synchronization. IEEE Trans Power Syst. 2018;33(4):4604–4613. https://doi.org/10.1109/TPWRS.2018.2790390.

[56] Schwarz G. Estimating the dimension of a model. Ann Statist. 1978;6(2):461–464. https://doi.org/10.1214/aos/1176344136.

[57] Akaike H. A new look at the statistical model identification. IEEE Trans Autom Control. 1974;19(6):716–723. https://doi.org/10.1109/TAC.1974.1100705.

[58] Huber PJ. Robust estimation of a location parameter. Ann Math Stat. 1964;35(1):73–101. https://doi.org/10.1214/aoms/1177703732.